Cell competition acts as a purifying selection to eliminate cells with mitochondrial defects during early mouse development

Ana Lima[1,2,#] Gabriele Lubatti[3,4,5,#], Jörg Burgstaller[6], Di Hu[7], Alistair Green[8], Aida Di Gregorio[1], Tamzin Zawadzki[1], Barbara Pernaute[1,9], Elmir Mahammadov[3,4,5], Salvador Perez Montero[1], Marian Dore[2], Juan Miguel Sanchez[1], Sarah Bowling[1], Margarida Sancho[1], Mohammad Karimi[2,10], David Carling[2], Nick Jones[8], Shankar Srinivas[7], Antonio Scialdone[3,4,5,11,*] and Tristan A. Rodriguez[1,11,*]

[1] National Heart and Lung Institute, Imperial College London, UK

[2] MRC London Institute of Medical Sciences (LMS), Institute of Clinical Sciences, Imperial College London, UK

[3] Institute of Epigenetics and Stem Cells, Helmholtz Zentrum München, Munich, Germany

[4] Institute of Functional Epigenetics, Helmholtz Zentrum München, Neuherberg, Germany

[5] Institute of Computational Biology, Helmholtz Zentrum München, Neuherberg, Germany

[6] Institute of Animal Breeding and Genetics, University of Veterinary Medicine, Vienna, Austria

[7] Department of Physiology, Anatomy and Genetics, University of Oxford, Oxford, UK

[8] Department of Mathematics, Imperial College London, UK.

[9] Current address: Centre for Genomic Regulation (CRG), The Barcelona Institute of Science and Technology, Dr. Aiguader 88, Barcelona 08003, Spain

[10] Current address: Comprehensive Cancer Centre, School of Cancer & Pharmaceutical Sciences, Faculty of Life Sciences & Medicine, King's College London, Denmark Hill, London SE5 9NU, UK.

[11] These authors jointly supervised this work.

[#] Both these authors contributed equally

* Authors for correspondence: antonio.scialdone@helmholtz-muenchen.de;

tristan.rodriguez@imperial.ac.uk

Abstract

Cell competition is emerging as a quality control mechanism that eliminates unfit cells in a wide range of settings from development to the adult. However, the nature of the cells normally eliminated by cell competition and what triggers their elimination remains poorly understood. In mouse, prior to gastrulation 35% of epiblast cells are eliminated. Here we have performed single cell transcriptional profiling of these cells and find that they show the hallmarks of cell competition and have mitochondrial defects. We demonstrate that mitochondrial defects are common to a range of different loser cell types and that manipulating mitochondrial function is sufficient to trigger competition. Importantly, we show that in the embryo cell competition eliminates cells with mitochondrial DNA mutations and that even non-pathological changes in mitochondrial DNA sequence can induce cell competition. Our results therefore suggest that cell competition is a purifying selection that optimises mitochondrial performance prior to gastrulation.

Running title: Cell competition and mitochondrial selection

Keywords: mitochondria, mtDNA, mouse development, cell competition, purifying selection

1   Cell competition is a fitness sensing mechanism that eliminates cells that, although viable, are

2   less fit than their neighbours. The cells that are eliminated are generically termed losers, while

3   the fitter cells that survive are referred to as winners. Cell competition has been shown to act in

4   a broad range of settings, from the developing embryo to the ageing organisms[1-3]. It has been

5   primarily studied in *Drosophila*, where it was first described in the imaginal wing disc [4]. Since

6   then, it has also been found to be conserved in mammals. In the mouse embryo 35% of

7   embryonic cells are eliminated between E5.5 and E6.5 and there is strong evidence that this

8   elimination is through cell competition[5-7]. These and other studies identified a number of read-

9   outs of cell competition in the mouse embryo, such as relative low c-MYC expression, a loss of

10   mTOR signalling, low TEAD activity, high P53 expression, or elevated levels of ERK

11   phosphorylation [5-9]. Importantly, there is a significant overlap with the markers of cell competition

12   originally identified in *Drosophila* as well as those found in other cell competition models, such

13   as Madin-Darby Canine Kidney (MDCK) cells – as reviewed[1-3]. In spite of the advance that

14   having these cell competition markers signifies, given that they were primarily identified by using

15   genetic models that rely on over-expression or mutation, we still have little insight into the over-

16   arching features of the cells that are eliminated in the physiological context.

17   Mitochondria, with their diverse cellular functions ranging from determining the bioenergetic

18   output of the cell to regulating its apoptotic response, are strong candidates for determining

19   competitive cell fitness. During early mouse development mitochondria undergo profound

20   changes in their shape and activity[10]. In the pre-implantation embryo mitochondria are rounded,

21   fragmented and contain sparse cristae, but upon implantation they fuse to form complex

22   networks with mature cristae[11]. The mode of replication of the mitochondrial genome (mtDNA),

23   that encodes for vital components of the bioenergetic machinery, also changes during early

24   mouse development. After fertilization, mtDNA replication ceases and its copy number per cell

25   decreases with every division until post-implantation stages, when mtDNA replication resumes[10].

26   As the mutation rate of mtDNA is significantly higher than that of nuclear DNA[12, 13], this

27   increased replication most likely leads to an increased mutation load. In fact, inheritable mtDNA

4

28   based diseases are reported with a prevalence of 5-15 cases per 100,000 individuals[14, 15]. A

29   number of mechanisms have been proposed to reduce this mutation load, such as the

30   bottleneck effect, purifying selection or biased segregation of mtDNA haplotypes[16-21]. However,

31   how these mechanisms act at the molecular and cellular level is still poorly understood.

32   To understand the nature of the cells eliminated during early mouse post-implantation

33   development, we have analysed their transcriptional profile by single-cell RNA sequencing and

34   found that these cells share a cell competition signature. Analysis of the pathways mis-regulated

35   identified mitochondrial dysfunction as a common feature. Importantly, our studies uncovered

36   that the cells eliminated have mtDNA mutations. Furthermore, we demonstrate that manipulating

37   mitochondrial activity either by disrupting mitochondrial dynamics or by introducing non-

38   pathological mtDNA changes is sufficient to trigger cell competition. These results therefore

39   pinpoint mitochondrial performance as a key cellular feature that determines the competitive

40   ability of embryonic cells and suggest that cell competition is acting as a purifying selection

41   during early mammalian development.

42

Results

44   **Cells eliminated in the early mouse embryo have a distinct transcriptional profile**

45   We have previously shown that in the early post-implantation mouse embryo about 35% of

46   epiblast cells are eliminated and that these cells are marked by low mTOR signalling[7]. However,

47   we currently do not understand the characteristics of these cells or what triggers their

48   elimination. To answer these questions, we have analysed their transcriptional profile by single

49   cell RNA sequencing (scRNA-seq). To ensure we can capture the eliminated cells, as we have

50   done before[7], we isolated embryos at E5.5 and cultured them for 16 hours in the presence of a

51   caspase inhibitors (CI) or vehicle (DMSO) (Fig. 1a). Unsupervised clustering of the scRNA-seq

52   data revealed five clusters: two corresponding to extra-embryonic tissues (visceral endoderm

53   and extra-embryonic ectoderm) and three that expressed epiblast marker genes (Fig. 1b-c,

54   Extended Data Fig. 1a-f and Methods). Interestingly, cells from CI- and DMSO-treated embryos

55   are unequally distributed across the three epiblast clusters. In particular, one of these clusters

56   (cluster 4) is only composed of cells from CI-treated embryos (Fig. 1d-e). It is worth noting that

57   all epiblast clusters contained cells in G2/M and S phases of the cell cycle, suggesting they are

58   all cycling (Extended Data Fig. 2a).

59   The three epiblast clusters are highly connected, as highlighted by a connectivity analysis

60   carried out with PAGA[22] (Extended Data Fig. 2b). Hence, to establish the relationship between

61   these epiblast clusters we computed a diffusion map[23]. For this, we selected only cells captured

62   from CI-treated embryos, to eliminate possible confounding effects due to the caspase inhibitor

63   (Fig. 2a). However, when all epiblast cells are considered, the results remain unchanged

64   (Extended Data Fig. 2c-e). This analysis identified a trajectory between the three epiblast

65   clusters, with those cells unique to CI-treated embryos falling at one extreme end of the

66   trajectory (corresponding to cluster 4; Fig. 2a) and with those cells present in both DMSO and

67   CI-treated embryos at the other (corresponding to cluster 1; Fig. 2a and Extended Data Fig. 2d).

68   To further define the identity of the epiblast cells of CI-treated embryos we analysed the genes

69   differentially expressed along the trajectory (see Methods and Extended Data Fig. 3a) using

70   Ingenuity Pathway Analysis (IPA) to characterize gene signatures[24]. Importantly, we found that

71   these differentially expressed genes fell under molecular and cellular function categories

72   associated with cell death and survival, protein synthesis and nucleic acids (Fig. 2b). Analysis of

73   the factors with enriched targets within the genes differentially expressed along the trajectory

74   revealed RICTOR (an mTOR component), TLE3, MYC, MYCN, P53 and IGFR (that is upstream

75   of mTOR) as the top upstream regulators (Fig. 2c). Breaking down the differentially expressed

76   genes into those down-regulated or up-regulated along the winner-to loser trajectory revealed

77   that the targets of RICTOR, MYC, MYCN and IGFR primarily fell within the down-regulated

78   genes (Supplementary Tables 1 and 2). P53 activated targets were preferentially up-regulated

79   and P53 repressed targets were preferentially down-regulated (Extended Data Fig. 3b-c).

80   Moreover, genes related to protein synthesis were primarily found to be downregulated.

81   The observation that the genes differentially expressed along the trajectory fall into cell death

82   categories, as well as being mTOR, MYC and P53 targets strongly suggests that cells at each

83   end of the trajectory are the winners and losers of cell competition[5-7]. For this reason, we

84   hereafter refer to those epiblast cells unique to CI-treated embryos as "loser" epiblast cells and

85   to those at the opposite end of the trajectory as the "winner" epiblast cells. Those cells lying

86   between these two populations on the trajectory are considered "intermediate". Using this

87   knowledge we can define a diffusion pseudotime (dpt) coordinate[25] originating in the "winner"

88   cluster that tracks the position of cells along the trajectory and that can be interpreted as a

89   "losing score", i.e., it quantifies how strong the signature of the "losing" state is in the

90   transcriptome of a cell (see Fig. 2d-e).

91   In accordance with previous studies[6, 8, 9], we also found evidence for miss-patterning in the

92   eliminated epiblast cells, as a proportion of these cells co-expressed naïve pluripotency and

93   differentiation markers (Fig. 2f and Extended Data Fig. 3d). To test if loser cells are

94   developmentally delayed or advanced compared to control cells we projected our data onto a

95   previously published diffusion map that includes epiblast cells from E5.5, E6.25 and E6.5 stage

96   embryos[26]. We found that all epiblast cells, irrespective of the condition the embryos were

97   cultured in (ie, DMSO or CI-treated) and of their losing state (ie, that they belonged to the

98   winner, intermediate or loser cluster) mostly overlap with the E6.5 epiblast cells (Extended data

99   Fig. 3e-g). Cells from the loser cluster are slightly closer to the E6.25 stage than the winner and

100 intermediate cells, as shown by their pseudo-time coordinate, but they remain far from the earlier

101 E5.5 stage. This result combined with the higher expression of some differentiation markers

102 observed in loser cells suggests that these cells are miss-patterned rather than developmentally

103 delayed.

104 **Loser cells are characterised by defects in mitochondrial function**

105 We next analysed using IPA the cellular pathways mis-regulated in loser epiblast cells and found

106 that the top two pathways (mitochondrial dysfunction and oxidative phosphorylation) are related

107 to mitochondrial function (Fig. 3a-b, Supplementary Table 1 and 2). For example, we found a

108   down-regulation along the winner to loser trajectory of the mtDNA encoded *mt-Nd3* and *mt-Atp6*,

109   of regulators of mitochondrial dynamics such as *Opa1,* as well as of genes involved in

110   mitochondrial membrane and cristae organisation such as *Samm50* (Fig. 3c), suggesting that

111   mitochondrial function is impaired in loser cells.

112   A recent body of evidence has revealed that stress responses, such as the integrated stress

113   response (ISR) or the closely related unfolded protein response (UPR), when triggered in cells

114   with impaired mitochondrial function prompt a transcriptional program to restore cellular

115   homeostasis[27-29]. We observed that loser epiblast cells displayed a characteristic UPR-ISR

116   signature[30-33] and key regulators of this response, such as *Atf4, Ddit3*, *Nrf2* and *Foxo3* were all

117   up-regulated in these cells (Extended Data Fig. 4a-d). Similarly, *Sesn2*, a target of p53 that

118   controls mTOR activity[34], was also up-regulated in loser cells (Extended Data Fig. 4d). These

119   findings support that loser epiblast cells present mitochondrial defects, leading to the activation

120   of a stress response in an attempt to restore cellular homeostasis[35].

121   To validate the significance of the observed mitochondrial defects, we did two things. First, we

122   asked if the changes of mitochondrial regulators at the mRNA level are also reflected at the

123   protein level. We observed that in CI-treated embryos, loser cells that persist and are marked by

124   low mTOR activity[7], also show significantly lower OPA1 levels (Fig. 3d-f). We also found that

125   DMSO-treated embryos showed strong DDIT3 staining (an UPR-ISR marker) in the dying cells

126   that accumulate in the proamniotic cavity, and that in CI-treated embryos, DDIT3 expression was

127   up-regulated in a proportion of epiblast cells (Extended Data Fig. 4e-g). The second thing we did

128   to validate the importance of the mitochondrial defects was to study in loser epiblast cells their

129   mitochondrial membrane potential ($\Delta\psi$m), an indication of mitochondrial health. We observed

130   that while the cells of DMSO-treated embryos showed a high $\Delta\psi$m that fell within a narrow

131   range, in CI-treated embryos the proportion of cells with a low $\Delta\psi$m significantly increased (Fig.

132   3d and 3g-h). Together, these results suggest that loser epiblast cells have impaired

133   mitochondrial activity that triggers a stress response.

134   **Mitochondrial dysfunction is common to different types of loser cells**

135   To address if mitochondrial defects are a common feature of loser cells eliminated by cell

136   competition, we analysed ESCs that are defective for BMP signalling (*Bmpr1a*^{-/-}) and tetraploid

137   cells (4n)[6]. We first carried out a mass spectrometry analysis using the Metabolon platform and

138   found that metabolites and intermediates of the TCA cycle, such as malate, fumarate, glutamate

139   and α-ketoglutarate are depleted in both *Bmpr1a*^{-/-} and 4n ESCs in differentiation culture

140   conditions (Fig. 4a). Next, we performed an extracellular flux Seahorse analysis of *Bmpr1a*^{-/-}

141   ESCs to measure their glycolytic and oxidative phosphorylation (OXPHOS) rates. We observed

142   that when these cells are maintained in pluripotency culture conditions that are not permissive

143   for cell competition[6], they showed a similar glycolytic activity but a higher OXPHOS rate than

144   control cells (Extended Data Fig. 5a-b). In contrast, when *Bmpr1a*^{-/-} cells are induced to

145   differentiate, this phenotype is reversed, with mutant cells showing lower ATP generated through

146   OXPHOS and a higher glycolytic capacity than controls (Fig. 4b-e and Extended Data Fig. 5c-d).

147   This suggests that upon differentiation *Bmpr1a*^{-/-} cells are unable to sustain proper OXPHOS

148   activity.

149   To further test the possibility that defective ESCs have impaired mitochondrial function, we

150   assessed their $\Delta\psi m$. We found that whilst *Bmpr1a*^{-/-} and 4n cells had a similar $\Delta\psi m$ to control

151   cells in pluripotency conditions (Extended Data Fig. 5e-f), upon differentiation both these cell

152   types presented a loss of $\Delta\psi m$, irrespective of whether they were separate or co-cultured with

153   wild-type cells (Fig. 4f-g). This reduction in $\Delta\psi m$ is not due to excessive mitochondrial reactive

154   oxygen species (ROS) production or to a lower mitochondrial mass within mutant cells since, as

155   for example, *Bmpr1a*^{-/-} cells have lower ROS levels and similar TOMM20 and mt-CO1

156   expression as control cells (Fig. 4h-j and Extended Data Fig. 5g). The fact that the loss of $\Delta\psi m$

157   and lower OXPHOS activity can be observed even when loser cells are cultured separately,

158   suggests that the mitochondrial dysfunction phenotype is an inherent property of loser cells and

159   not a response to them being out-competed. These results also indicate that the mitochondrial

160   defects are directly linked to the emergence of the loser status: in conditions that are not

161   permissive for cell competition (pluripotency) mutant cells do not show defective mitochondrial

162   function, but when they are switched to differentiation conditions that allow for cell competition,

163   they display impaired mitochondrial function.

164   To further explore the relationship between mitochondrial activity and the competitive ability of

165   the cell, we analysed the Δψm of BMP defective cells that are null for p53 (*Bmpr1a^-/-^; p53^-/-^*

166   ESCs), as these are not eliminated by wild-type cells[7]. Remarkably, we observed that mutating

167   *p53* in *Bmpr1a^-/-^* cells not only rescues the loss of Δψm of these cells, but also causes

168   hyperpolarisation of their mitochondria (Fig. 4k). These results not only suggest a role for P53 in

169   regulating mitochondrial activity of ESCs, but also strongly support a pivotal role for

170   mitochondrial activity in cell competition.

171   **Impaired mitochondrial function is sufficient to trigger cell competition**

172   The mitochondrial defects observed in loser cells led us to ask if disrupting mitochondrial activity

173   alone is sufficient to trigger cell competition. During the onset of differentiation, mitochondrial

174   shape changes substantially. In pluripotent cells mitochondria have a round and fragmented

175   shape, but upon differentiation they fuse and become elongated, forming complex networks[10].

176   Given that this change in shape correlates with when cell competition occurs, we tested if

177   disrupting mitochondrial dynamics is sufficient to induce cell competition. MFN1 and MFN2

178   regulate mitochondrial fusion and DRP1 controls their fission[36-38]. We generated *Mfn2^-/-^* ESCs,

179   that have enlarged globular mitochondria, and *Drp1^-/-^* ESCs, that show hyper-elongated

180   mitochondria (Fig. 5a). We observed that *Mfn2^-/-^* ESCs displayed very poor growth upon

181   differentiation (data not shown). For this reason, we tested their competitive ability in

182   pluripotency conditions, that we have previously found not to induce the out-competition of

183   *Bmpr1a^-/-^* or 4n cells[6]. Interestingly, we found that although *Mfn2^-/-^* cells grow similarly to wild-

184   type cells in separate cultures, they were out-competed in co-culture (Fig. 5b). Analysis of the

185   *Drp1* mutant cells showed that although they did not grow significantly slower than wild-type

186   cells when cultured separately in differentiation inducing conditions, they were out-competed by

187   wild-type cells in co-culture (Fig. 5c). The observation that disrupting mitochondrial dynamics

10

188   can induce cell competition even in pluripotency culture conditions, suggests that mitochondrial

189   activity is a dominant parameter determining the competitive ability of the cell.

190   To establish how disruption of mitochondrial fusion and fission affects mitochondrial

191   performance we compared the Δψm, respiration rates and mitochondrial ATP production of

192    $Mfn2^{-/-}$ and $Drp1^{-/-}$ ESCs to that of wild-type cells (Fig. 5d-g). We found that whilst $Mfn2^{-/-}$ and

193    $Drp1^{-/-}$ ESCs had lower Δψm than control cells (Fig. 5d,f), $Mfn2^{-/-}$ ESCs had lower maximal

194   respiration rates but similar basal respiration and ATP production to controls and $Drp1^{-/-}$ ESCs

195   showed similar respiration and ATP production to controls (Fig. 5e,g). This suggests that ATP

196   production or respiration rates alone do not determine the relative competitive ability of ESCs.

197   Besides mitochondrial dysfunction, another prominent signature of loser cells found *in vivo* was

198   the UPR/ISR (Ext. Data Fig. 4). Since the loss of *Drp1* has been associated with activation of the

199   UPR[39-41], we investigated if the $Drp1^{-/-}$ loser cells also showed evidence for the activation of the

200   UPR/ISR. We observed that $Drp1^{-/-}$ cells show higher expression of ATF4 and p-eIF2α than wild-

201   type counterparts, which is indicative of UPR/ISR activation (Fig. 5h)[39-41]. Another feature

202   previously described upon loss of *Drp1* is the proteolytic cleavage of OPA1, where short

203   isoforms (S-OPA1) are accumulated in detriment of the long isoforms (L-OPA1)[39]. When we

204   analysed the expression of OPA1 in wild-type and $Drp1^{-/-}$ cells we observed that while wild-type

205   cells retain L-OPA1 expression, loser cells predominantly express the S-OPA1 isoforms and

206   display almost no expression of L-OPA1 (Fig. 5i). This defect has been associated with mito-

207   ribosomal stalling, a phenotype that can be replicated by treating cells with actinonin (Extended

208   Data Fig. 6)[42]. To test if the shift in isoform expression observed in $Drp1^{-/-}$ ESCs is due to

209   aberrant mitochondrial translation we treated cells with doxycycline, that inhibits this

210   translation[43], and observed that this was sufficient to partially rescue L-OPA1 expression (Fig.

211   5j). This rescue together with the evidence for UPR/ISR expression suggest that $Drp1^{-/-}$ cells

212   display defects in mitochondrial translation.

213   **Loser epiblast cells accumulate mtDNA mutations**

11

214   There is strong evidence for selection against aberrant mitochondrial function induced by

215   deleterious mtDNA mutations in mammals[21, 44-47]. Given that we observe that cell competition

216   selects against cells with impaired mitochondrial function, we asked if cell competition could be

217   reducing mtDNA heteroplasmy (frequency of different mtDNA variants) during mouse

218   development. It has been recently shown that scRNA-seq can be used to reliably identify mtDNA

219   variants, although with a lower statistical power compared to more direct approaches, like

220   mtDNA sequencing[48]. We therefore tested if mtDNA heteroplasmy is present in our scRNA-seq

221   data and whether this correlates with the losing score of a cell. Our analysis revealed that the

222   frequency of specific mtDNA polymorphisms increased with the losing score of epiblast cells

223   (Fig. 6a), and such mtDNA changes occurred within *mt-Rnr1* and *mt-Rnr2* (Fig. 6b-h and

224   Extended Data Fig. 7a-e). Moreover, these changes were not dependent on the litter from which

225   the embryo came from (Extended Data Fig. 7f-k). The mutations we detected in *mt-Rnr1* and *mt-*

226   *Rnr2* strongly co-occurred in the same cell, with those closest together having the highest

227   probability of co-existing (Fig. 6i and Extended Data Fig. 7l). This is suggestive of mtDNA

228   replication errors that could be 'scarring' the mtDNA, disrupting the function of *mt-Rnr1* (12S

229   rRNA) and *mt-Rnr2* (16S rRNA) and causing the loser phenotype. Importantly, the presence of

230   these specific mtDNA mutations in the loser cells suggests that cell competition is contributing to

231   the elimination of deleterious mtDNA mutations during early mouse development.

232   **Changes in mtDNA sequence can determine the competitive ability of a cell**

233   To explore this possibility further, we analysed if alterations in mtDNA can induce cell

234   competition by testing the competitive ability of ESCs with non-pathological differences in

235   mtDNA sequence. For this we compared the relative competitive ability of ESCs that shared the

236   same nuclear genome background but differed in their mitochondrial genomes by a small

237   number of non-pathological sequence changes. We derived ESCs from hybrid mouse strains

238   that we had previously engineered to have a common nuclear C57BL/6N background, but

239   mtDNAs from different wild-caught mice[16]. Each wild-derived mtDNA variant (or haplotype)

240   contains a specific number of single nucleotide polymorphisms (SNPs) that lead to a small

12

241   number of amino acid changes when compared to the C57BL/6N mtDNA haplotype.

242   Furthermore, these haplotypes (BG, HB and ST) can be ranked according to their genetic

243   distance from the C57BL/6N mtDNA (Fig. 7a and Extended Data Fig. 8a). Characterization of

244   the isolated ESCs revealed that they have a range of heteroplasmy (mix of wild-derived and

245   C57BL/6N mtDNAs) that is stable over several passages (Extended Data Fig. 8b). Importantly,

246   these different mtDNA haplotypes and different levels of heteroplasmy do not alter cell size, cell

247   granularity, mitochondrial mass or mitochondrial dynamics, nor do they substantially impact the

248   cell's Δψm (Extended Data Fig. 8c-f).

249   When we tested the competitive ability of these ESCs with different mtDNA content, in

250   pluripotency culture conditions, we observed that cells carrying the mtDNAs that are most distant

251   from the C57BL/6N mtDNA, such as the HB(100%), the HB(24%) and the ST(46%) ESCs could

252   all out-compete the C57BL/6N line (Fig. 7b-c and Extended Data Fig. 8g). Similarly, when we

253   tested the HB(24%) line against the BG(99%) or the BG(95%) lines (that have mtDNAs more

254   closely related to the C57BL/6N mtDNA), we found that cells with the HB haplotype could also

255   out-compete these ESCs (Fig. 7d and Extended Data Fig. 8h). In contrast, we observed that the

256   HB(24%) ESCs were unable to out-compete either their homoplasmic counterparts, HB(100%),

257   or the ST(46%) cells that carry the most distant mtDNA variant from C57BL/6N (Fig. 7e and

258   Extended Data Fig. 8i). These results tell us three things. First, that non-pathological differences

259   in mtDNA sequence can trigger cell competition. Second, that a competitive advantage can be

260   conferred by only a small proportion of mtDNA content, as indicated by our finding that HB(24%)

261   behave as winners. Finally, these findings suggest that the phylogenetic proximity between

262   mtDNA variants can potentially determine their competitive cell fitness.

263   To characterise the mode of competition between cells with different mtDNA we focussed on the

264   HB(24%) and the BG(95%) ESCs. Analysis of these cell lines revealed that specifically when co-

265   cultured, the BG(95%) cells display high levels of apoptosis (Fig. 7f), indicating that their out-

266   competition is through their elimination. To gain further insight we performed bulk RNA-seq of

267   these cells in separate and co-culture conditions (Extended Data Fig. 8j) and analysed the

13

268   differentially expressed genes by gene-set enrichment analysis (GSEA). We found that in

269   separate culture the most notable features that distinguish BG(95%) from HB(24%) cells were a

270   down-regulation of genes involved in oxidative phosphorylation and an up-regulation of those

271   associated with cytokine activity (Fig. 8g). Interestingly, in the co-culture condition, in addition to

272   these signatures, BG(95%) cells revealed a down-regulation in signature markers of MYC

273   activity and mTOR signalling (Fig. 7h), whose downregulation are known read-outs of a loser

274   status during cell competition in the embryo[5-7] (Fig. 2c).

275   To test if the down-regulation of genes involved in oxidative phosphorylation was also reflected

276   at the functional level we compared oxygen consumption rates and mitochondrial ATP

277   generation in HB(100%), HB(24%), BG(95%) and C57Bl/6N ESCs. We find that the winner cells

278   HB(100%) and HB(24%) have higher basal respiration, higher maximal respiration and higher

279   mitochondrial ATP production than the loser BG(95%) and C57BL/6N ESCs (Extended Data Fig.

280   9). These data indicate that the mtDNA differences that exist between winner and loser cells are

281   sufficient to affect their mitochondrial performance and this ultimately determines their

282   competitive ability. However, the observation that differentiating $Drp1^{-/-}$ ESCs are eliminated by

283   cell competition but do not show differences in respiration rates or mitochondrial ATP production

284   (Fig. 5b,e), suggests that respiration or ATP production rates alone are unlikely to be the

285   mitochondrial parameters that control competitive cell fitness.

286   The finding that the genes down-regulated in BG(95%) cells when co-cultured with HB(24%)

287   cells fell under functional categories relating to mitochondrial function (Extended Data Fig. 10a)

288   led us to analyse the degree of overlap between these genes and the genes differentially

289   expressed along the winner-to-loser trajectory in the embryo. We observed a significant overlap

290   in mis-regulated genes (Extended Data Fig. 10b), as well as in the functional components that

291   these genes can be categorised into (Extended Data Fig. 10c). This further highlights the

292   importance of relative mitochondrial activity for determining the competitive ability of embryonic

293   cells.

14

Discussion

The emerging role of cell competition as a regulator of cell fitness in a wide range of cellular contexts, from the developing embryo to the ageing tissue[1-3], has highlighted the importance of understanding what cell types are normally eliminated by this process. With the aim of understanding this question, we have analysed the transcriptional identity of the cells eliminated in the early mouse embryo. We have found not only that they present a cell competition signature but also that they are marked by mtDNA mutations and impaired mitochondrial function. Starting from these results, we leveraged *in vitro* models of cell competition to show that: (i) mitochondrial function is impaired in loser cells eliminated by cell competition, and (ii) differences in mitochondrial activity are sufficient to trigger cell competition in ESCs. Overall, this points to mitochondrial performance as a key determinant of the competitive ability of cells during early mammalian embryonic development. One implication of our findings is that a range of different types of defects, such as mis-patterning, karyotypic abnormalities or mtDNA mutations, all lead to dysfunctional mitochondria at the onset of differentiation and that ultimately it is their impaired mitochondrial function that triggers cell competition, inducing their elimination (Fig. 8).

Embryos are exposed to different microenvironments in vivo and when cultured ex-vivo. Similarly, ESCs also experience a different micro-environment to epiblast cells in the embryo. These different micro-environments could potentially affect the selective pressure and hence the transcriptional signature of loser cells. However, there are two reasons why we think that the loser cell signatures we identify here are conserved across systems. First, the transcriptional profile of our epiblast cells from cultured embryos is very similar to that of epiblast cells from freshly isolated embryos (see Extended Data Figure 3e-g). Second, the loser signature identified here is enriched for targets of P53 and depleted for mTOR and c-MYC targets. Given that these are regulators of cell competition identified by us and others in the embryo and in ESCs[5-7], it suggests that the same pathways are inducing loser cell elimination in in vivo, ex-vivo and in ESC models of cell competition.

15

321   It is well known that the successful development of the embryo can be influenced by the quality

322   of its mitochondrial pool[10]. Moreover, divergence from normal mitochondrial function during

323   embryogenesis is either lethal or can lead to the development of mitochondrial disorders[49].

324   Deleterious mtDNA mutations are a common cause of mitochondrial diseases and during

325   development selection against mutant mtDNA has been described to occur through at least two

326   mechanisms: the bottleneck effect and the intra-cellular purifying selection. The bottleneck effect

327   is associated specifically with the unequal segregation of mtDNAs during primordial germ cell

328   specification, for example as seen in the human embryo[50]. In contrast to this, purifying selection,

329   as the name implies, allows for selection against deleterious mtDNAs and has been proposed to

330   take place both during development and post-natal life[51]. Importantly, purifying selection has

331   been found to occur at the molecule and organelle level, as well as at the cellular level[52]. Our

332   findings indicate that purifying selection can occur not only at the intra-cellular level but also

333   inter-cellularly (cell non-autonomously). We show that epiblast cells are able to sense their

334   relative mitochondrial activity and that those cells with mtDNA mutations, lower or aberrant

335   mitochondrial function are eliminated. By selecting those cells with the most favourable

336   mitochondrial performance, cell competition would not only prevent cells with mitochondrial

337   defects from contributing to the germline or future embryo, but also ensure optimisation of the

338   bioenergetic performance of the epiblast, therefore contributing to the synchronization of growth

339   during early development.

340   Cell competition has been studied in a variety of organisms, from *Drosophila* to mammals, and it

341   is likely that multiple different mechanisms fall under its broad umbrella[1-3]. In spite of this, there

342   is considerable interest in understanding if there could be any common feature in at least some

343   of the contexts where cell competition has been described. The first demonstration of cell

344   competition in *Drosophila* was made by inducing clones carrying mutations in the ribosomal

345   gene *Minute*[4] and this has become one of the primary models to study this process. Our finding

346   that during normal early mouse development cell competition eliminates cells carrying mutations

347   in *mt-Rnr1* and *mt-Rnr2*, demonstrates that in the physiological context mutations in ribosomal

16

348   genes also trigger cell competition. Furthermore, our observation that mis-patterned and

349   karyotypically abnormal cells show impaired mitochondrial activity indicates that during early

350   mouse development different types of defects impair mitochondrial function and trigger cell

351   competition. Interestingly, mtDNA genes are amongst the top mis-regulated factors identified

352   during cell competition in the mouse skin[53]. In the *Drosophila* wing disc oxidative stress, a

353   general consequence of dysfunctional mitochondria, underlies the out-competition of *Minute* and

354   *Mah-jong* mutant cells[54]. Similarly, in MDCK cells a loss of $\Delta\psi m$ occurs during the out-

355   competition of RasV12 mutant cells and is key for their extrusion[55]. These observations raise the

356   possibility that differences in mitochondrial activity may be a key determinant of competitive cell

357   fitness in a wide range of systems. Unravelling what mitochondrial features can lead to cellular

358   differences that can be sensed between cells during cell competition and if these are conserved

359   in human systems will be key not only for understanding this process, but also to open up the

360   possibility for future therapeutic avenues in the diagnosis or prevention of mitochondrial

361   diseases.

Acknowledgments

17

Author Contributions

375   A.L. performed most of the experimental wet lab work. J.B. and A.L. derived heteroplasmic

376   mESC lines. J.B. performed heteroplasmy measurements in heteroplasmic mESCs. B.P.

377   generated $Mfn2^{-/-}$ and $Drp1^{-/-}$ mESCs and J.M.S did characterisation of mitochondria shape and

378   pluripotency status. S.P.M participated in the metabolic characterisation of $Drp1^{-/-}$ cells. D.H.

379   performed embryo dissections, treatments and cell dissociation prior to scRNA-seq experiments.

380   G.L. did the bioinformatic analysis of scRNA-seq data. E.M., N.J. and A.G. participated in the

381   analysis of mitochondrial DNA heteroplasmy. A.D.G. performed the metabolomic studies using

382   Metabolon platform and participated in embryo dissections and immunohistochemistry stainings

383   for validation of results obtained by scRNA-seq. M.D, and M.K. performed the bioinformatic

384   analysis of bulk RNA-seq experiments. N.J., S.S. and D.C. participated in the design of

385   experimental work and analysis of results. A.L., G.L., A.S and T.R. interpreted results and wrote

386   the paper. T.R. and A.S. directed and designed the research.

Competing Interests

388   The authors declare no competing interests.

Figure titles and legends

Fig. 1 | Cells eliminated during early mouse embryogenesis have a distinct transcriptional profile.

a, Experimental design. The number of cells in the two conditions (DMSO-treated and CI-treated) refers to the number of cells that passed the quality control. **b**, Identification of the clusters according to known gene markers from the different embryonic regions[56]. Three clusters (clusters 1, 3 and 4) show marker genes of the epiblast (Epi), while the remaining clusters correspond to the extra-embryonic lineages visceral endoderm (VE; cluster 5) and extraembryonic ectoderm (ExE; cluster 2). The epiblast clusters are named "Winner", "Intermediate" and "Loser" on the basis of the relative fraction of cells from CI-treated embryos they include (see panel **e**). **c,d**, UMAP visualization of the single-cell RNA-seq data, with cells coloured according to cluster (**c**) or condition (**d**). A region made up exclusively by cells from CI-treated embryos emerges. **e**, Ratio between the fraction of cells from DMSO-treated and CI-treated embryos in the three epiblast clusters. While the "winner" epiblast cluster shows an enrichment of cells from DMSO-treated embryos, the "intermediate" and the "loser" epiblast clusters are strongly enriched for cells from CI-treated embryos**.**

Fig. 2 | A cell competition transcriptional signature is identified in cells eliminated during mouse embryonic development.

a, Diffusion map of epiblast cells (only from CI-treated embryos), coloured by cluster. **b**, **c**, IPA run on the list of genes differentially expressed along the diffusion trajectory (see Extended Data Fig. 2a) generated lists of top 5 molecular and cellular functions (**b**) and upstream regulators (**c**) found to be differentially activated in epiblast cells along the diffusion trajectory from winner (cluster 1) to loser status (cluster 4). **d**, Diffusion map of epiblast cells (only from CI-treated embryos) coloured by diffusion pseudotime coordinate (dpt). The winner and the loser clusters are found at the two extremities of the trajectory, hence the dpt can be interpreted as a "losing score". **e**, Losing score of the cells in the three epiblast clusters in CI-treated (left) or DMSO-treated (right) embryos. The losing score of the cells from DMSO-treated embryos was obtained

417   by projecting them on the diffusion map shown in panel **d** (see Methods). **f,** Expression levels in

418   epiblast cells from CI-treated embryos of genes (in rows) that are markers for naïve pluripotency

419   (*Klf4, Klf5, Sox2, Pou3f1, Tcf7l1* and *Pou5f1 and Rex1*), primed pluripotency (*Fgf5* and *Tdgf1*),

420   mesoderm (*Mesp1* and *T*), neuroectoderm (*Neurod1* and *Sox1*) and endoderm (*Sox17 and*

421   *Gata6*). Cells (in columns) are sorted by their losing scores. The genes marked with a * are

422   differentially expressed along the trajectory.

423   **Fig. 3 | Cells eliminated during early mouse embryogenesis have mitochondrial defects.**

424   **a**, Top canonical pathways, identified by IPA, mis-regulated in loser cells in comparison to

425   normal epiblast cells. The numbers at the end of each bar refer to total amount of genes

426   involved in that pathway. The percentage refers to the number of genes found mis-regulated in

427   loser cells relative to the number total genes within each pathway. Statistical significance

428   calculated with Fisher's exact test (p<0.05): Mitochondrial Dysfunction, $-\log_{10}$(p-value) = 21.1;

429   Oxidative Phosphorylation, $-\log_{10}$(p-value) = 18.6; EIF2 signalling, $-\log_{10}$(p-value) = 11.9. **b**,

430   Detail of changes in oxidative phosphorylation pathway identified in (**a**). Circular and oval shapes

431   represent each of the ETC complexes (complexes I to V). Diamond shapes represent subunits

432   of each ETC complex. Genes that are down-regulated in loser cells are coloured in shades of

433   red. Darker shades correspond to lower values of FDR, which ranges from 1.25E-51 (for *Atp5b*)

434   to 5.42E-03 (for *Ndufa11*). *Cox6b2,* coloured in yellow, was found to be up-regulated in loser

435   cells (FDR=2.69E-13). Grey colour denotes genes that were not differentially expressed

436   between loser and winner cells (FDR>0.01). White colour denotes genes from the Knowledge

437   Base that were not tested (e.g., because they were not detected in our dataset). **c**, Expression

438   levels of some mitochondrial genes as a function of cells' losing score. *mt-Atp6*, mitochondrial

439   DNA encoded ATP synthase membrane subunit 6; *mt-Nd3*, mitochondrial DNA encoded NADH

440   dehydrogenase subunit 3; *Opa1*, optic atrophy 1; *Samm50*, sorting and assembly machinery

441   component 50 homolog. **d**, Experimental design adopted to assess mitochondria function (OPA1

442   expression, by immunofluorescence or Δψm, given by TMRM fluorescence) in epiblast cells

443   from embryos where cell death was allowed (DMSO-treated) or inhibited (CI-treated). *

444   Micrograph of isolated epiblast (arrow) after embryo microdissection. **e**, Representative

445   immunohistochemistry of OPA1 in E6.5 embryo where cell death was inhibited (CI-treated),

446   quantified in (**f**). Loser cells are identified by low mTOR activation (low p-rpS6, arrowheads).

447   Scale bar = 20 μm. **f**, Quantification of OPA1 fluorescence in normal epiblast cells and loser

448   cells. N=6 embryos with a minimum of 8 cells analysed per condition. Statistical analysis

449   performed by Mann-Whitney test. **g**, Representative histogram of flow cytometry analysis of

450   TMRM probe, indicative of Δψm, in epiblast cells from embryos where cell death was allowed

451   (DMSO-treated) or inhibited (CI-treated), quantified in (**h**). **h**, Frequency of epiblast cells with

452   high or low TMRM fluorescence, according to range defined in (**g**) from embryos where cell

453   competition was allowed (DMSO treated) or inhibited (CI-treated). Statistical analysis done by

454   two-way ANOVA, followed by Holm-Sidak's multiple comparisons test. N=3 independent

455   experiments. Data shown as mean ± SEM.

456   **Fig. 4 | Mitochondrial defects are a common feature of cells eliminated by cell**

457   **competition.**

458   **a**, Metabolic enrichment analysis of the TCA cycle and intermediate metabolites obtained using

459   Metabolon platform for defective cells (*Bmpr1a*^{-/-}, left bar and 4n, right bar), in comparison to

460   wild-type cells during differentiation. Bars indicate compound levels relative to wild-type cells.

461   Blue bars indicate compounds that are significantly depleted ($p < 0.05$) and light blue bars

462   indicate compounds that are almost significantly depleted ($0.05 \leq p \leq 0.1$). Black bars indicate

463   compounds that are depleted although not statistically significant in comparison to the levels

464   found in wild-type cells. The enzymes on the pathway are represented as boxes and labelled by

465   their canonical names. **b-e**, Metabolic flux analysis of wild-type and BMP-defective cells during

466   differentiating conditions. Data obtained with a minimum of 3 independent experiments, with 5

467   replicates per cell type in each assay. Statistical analysis done with Mann-Whitney test. Analysis

468   of oxygen consumption rate (OCR) as a measure of mitochondria function (mitochondria stress

469   test) (**b**). Detail of metabolic parameters found changed from the analysis of the mitochondria

470   stress test (**c**). Analysis of extracellular acidification rate (ECAR) as a measure of glycolytic

21

471   function (glycolysis stress test) (**d**). Detail of metabolic parameters found changed from the

472   analysis of the glycolysis stress test (**e**). **f-g**, Analysis of mitochondrial membrane potential

473   (Δψm) in defective mESCs undergoing differentiation in separate or co-culture conditions.

474   Representative histograms of TMRM fluorescence and quantification for wild-type and *Bmpr1a*$^{-/-}$

475   (**f**) and wild-type and 4n (**g**). Statistical analysis done by two-way ANOVA, followed by Holm-

476   Sidak's multiple comparisons test. **h**, Representative micrographs of wild-type and *Bmpr1a*$^{-/-}$

477   cells co-cultured during differentiation and stained for a reporter of Δψm (MitoTracker Red, top

478   panel) or mitochondria mass (TOMM20, bottom panel). Nuclei are stained with Hoechst. Scale

479   bar = 10 μm. **i-j**, Western blot analysis of mitochondria mass markers TOMM20 (**i**) and mt-CO1

480   (**j**) for wild-type and *Bmpr1a*$^{-/-}$ cells during differentiation. Statistical analysis done with Mann-

481   Whitney test (**i**) or unpaired t-test (**j**). **k**, Analysis of mitochondrial membrane potential (Δψm) for

482   wild-type, *Bmpr1a*$^{-/-}$ and *Bmpr1a*$^{-/-}$;*p53*$^{-/-}$ cells during differentiation. Representative histogram of

483   TMRM fluorescence and quantification. Statistical analysis done by one-way ANOVA, followed

484   by Holm-Sidak's multiple comparisons test. Data shown as mean ± SEM of a minimum of 3

485   independent experiments.

486   **Fig. 5 | Manipulating mitochondria biology is sufficient to trigger cell competition.**

487   **a**, Representative micrographs of wild-type*, Mfn2*$^{-/-}$ and *Drp1*$^{-/-}$ mESCs showing alterations in

488   mitochondrial morphology in mutant cells. TOMM20 was used as a mitochondrial marker and

489   NANOG as a pluripotency marker. Nuclei are stained with Hoechst. Scale bar = 5 μm. **b,c**, Cell

490   competition assays between wild-type mESCs and cells with altered morphology, *Mfn2*$^{-/-}$ during

491   pluripotency (**b**) and *Drp1*$^{-/-}$ during differentiation (**c**). The ratio of final/initial cell numbers in

492   separate or co-culture is shown. Statistical analysis done with two-way ANOVA, followed by

493   Holm-Sidak's multiple comparisons test. **d-j**, Metabolic profile of *Mfn2*$^{-/-}$ and *Drp1*$^{-/-}$ mESCs.

494   Analysis of mitochondrial membrane potential (Δψm) for wild-type and *Mfn2*$^{-/-}$ cultured

495   separately during pluripotency (**d**) and for wild-type and *Drp1*$^{-/-}$ mESCs $^{-/-}$ after 3 days of

496   differentiation in separate culture (**f**). Data was obtained from 3 independent experiments and

497   statistical testing done with one sample t-test. Metabolic flux analysis of wild-type and *Mfn2*$^{-/-}$

498   mESCs cultured separately during pluripotency (**e**) and for wild-type and *Drp1*^{-/-} after 3 days of

499   differentiation in separate cultures (**g**). Data was collected from 3 independent experiments, with

500   5 replicates per cell type in each assay, and statistical testing done with Mann-Whitney test. **h-j**,

501   Western blot analysis of markers of UPR and mitochondrial markers in wild-type and *Drp1*^{-/-} after

502   3 days of differentiation in separate culture. Cells were treated with doxycycline (Dox, 22.5 μM)

503   or vehicle (Con) from day 1 of differentiation and samples were collected on day 3 (**j**). Statistical

504   analysis was done with an unpaired t-test (h-i) or two-way ANOVA followed by Holm-Sidak's

505   multiple comparisons test (j). Data shown as mean ± SEM of a minimum of 3 independent

506   experiments. p-eIF2α, phosphorylated eukaryotic initiation factor 2α.

507   **Fig. 6 | Intermediate and loser epiblast cells accumulate polymorphisms in mtDNA**

508   **sequence.**

509   **a-g**, mtDNA heteroplasmy in epiblast cells from CI-treated embryos. Average heteroplasmy

510   (considering all eleven polymorphisms that have a statistically significant dependence on the

511   losing score; see Methods) as a function of cells' losing scores. The p-value was computed with

512   a generalized linear model (**a**). mtDNA heteroplasmy for six positions within the *mt-Rnr1* gene

513   (**b-g**). The heteroplasmy at all of these positions as well as the average heteroplasmy increase

514   with the cells' losing scores in a statistically significant way (the adjusted p-value estimated via a

515   generalized linear model is indicated at the top of each plot). **h**, The barplot indicates the fraction

516   of epiblast cells in each of the cluster indicated on the x-axis (winner, intermediate, loser) that

517   carry a mean heteroplasmy (computed on the six positions within the *mt-Rnr1* indicated in the

518   panels **b**-**g**) greater than 0.01. This shows that the level of mtDNA heteroplasmy in *mt-Rnr1* is

519   strongly associated with the loser status of the cells, since ~55% and ~87% of cells in the

520   intermediate and the loser clusters, respectively, have heteroplasmic sequences in this gene

521   compared to only ~5% of cells in the winner cluster. **i**, Spearman's correlation coefficient

522   between the mtDNA heteroplasmy at the six positions shown in panels (**b**-**g**).

523   **Fig. 7 | Changes in mtDNA sequence can determine the competitive ability of a cell.**

23

524   **a,** Derivation of mESCs from hybrid mouse strains, generated elsewhere by Burgstaller and

525   colleagues. Neighbour-Joining Phylogenetic Analysis of mtDNA from wild and C57BL/6N mouse

526   strains, that were used to generate hybrid mice (adapted from[16]), illustrates the genetic distance

527   of the mtDNA from wild mouse strains to the C57BL/6N lab mouse. The number of single

528   nucleotide polymorphisms and amino acid changes (SNPs/ a.a. changes) from wild to lab mouse

529   strain is shown. mESCs were derived from embryos of hybrid mice, containing the nuclear

530   background of a C57BL/6N lab mouse and mtDNA from three possible wild-derived strains (BG,

531   HB or ST). **b-e,** Cell competition assays between cells derived from the embryos of hybrid mice

532   performed in pluripotency maintenance conditions. The ratio of final/initial cell numbers in

533   separate or co-culture is shown. Statistical analysis done with two-way ANOVA, followed by

534   Holm-Sidak's multiple comparisons test. **f,** Representative micrographs of cleaved caspase-3

535   staining and quantification of the percentage of apoptotic events in winners HB(24%) and loser

536   BG(95%) mESCs maintained pluripotent and cultured in separate or co-culture conditions.

537   Statistical analysis done with two-way ANOVA, followed by Holm-Sidak's multiple comparisons

538   test. **g-h,** Gene set enrichment analysis of differentially expressed genes from bulk RNA seq. in

539   loser BG (95%) compared to winner HB (24%) mESCs maintained pluripotent and cultured in

540   separate (**g**) or co-culture conditions (**h**). Gene sets that show positive normalized enrichment

541   scores (NES) are enriched in loser cells, while gene sets that show negative NES are depleted

542   in loser cells. Data in panels (**b**-**f**) shown as mean ± SEM of a minimum of 3 independent

543   experiments.

544   **Fig. 8 | Model of cell competition.**

545   Summary of the main findings of the study. A range of cellular defects, such as aneuploidy, mis-

546   patterning or mtDNA mutations cause alterations in mitochondria function, which affect the

547   relative fitness of cells. The cells with suboptimal mitochondrial activity survive in a

548   homogeneous population but are eliminated by cell competition in the presence of fitter cells.

549   **Extended Data Fig. 1 | Quality controls of scRNA-seq and clustering robustness analysis.**

24

550   **a,** Selection criteria for quality control (QC) of all cells. A total of 723 passed the quality control

551   (723 good quality cells) and were considered for downstream analysis. All these parameters

552   were computed for each cell. Log_{10} total number of reads (top left): log_{10} of the sum of the

553   number of reads that were processed in every cell; Fraction of mapped reads (top central):

554   number of reads that are confidentially mapped to the reference genome divided by total number

555   of reads that were processed for each cell. This number is automatically provided by Salmon

556   v0.8.2; Fraction of genes (top right): number of reads mapped to endogenous genes divided by

557   the total sum of reads that were processed; Fraction of mt-genes (bottom left): number of reads

558   mapped to mitochondrial genes divided by the total sum of reads that were processed; Fraction

559   of spikes (bottom central): number of reads mapped to ERCC spike-ins divided by the total sum

560   of reads that were processed; Number of genes above 10 RPM (bottom right): number of genes

561   with expression level above 10 reads per million. **b,** Number of good quality cells in each

562   condition (rows) and batch (columns). **c,** Number of good quality cells per cluster (rows) and

563   batch (columns). **d,** UMAP plot of the data with cells coloured by batch. In each batch there is a

564   balanced distribution of cells in the two conditions and across the five clusters. **e,** The Pearson's

565   gamma (left panel) and the Average Silhouette Width (right panel) was calculated for each set of

566   clusters obtained with 100 random subsamples of 60% of highly variable genes and different

567   values of the deepSplit parameter (see Methods). The most robust clusters correspond to

568   deepSplit values of 0 and 1. **f,** The changes in composition and number of clusters between the

569   clustering obtained with deepSplit 0 (top) and 1 (bottom) are shown using the library "clustree"[57].

570   **Extended Data Fig. 2 | Cell cycle analysis and cluster connectivity.**

571   **a,** Cell cycle analysis of epiblast cells from clusters 1, 3 and 4. Cell cycle phase was predicted

572   with cyclone algorithm[58] and shows that there are cells in S and G2M phase also in the loser and

573   intermediate clusters. **b,** PAGA plot showing the connectivity of the five clusters of cells from CI-

574   treated embryos. **c-d,** Diffusion map analysis in all epiblast cells (from DMSO and CI-treated

575   embryos): cells are coloured according to the condition (**c**) and to the cluster (**d**). **e,** The pseudo-

576   time coordinate of the CI-treated epiblast cells obtained from the diffusion map including all

577   epiblast cells correlates extremely well with the pseudo-time coordinate obtained in the diffusion

578   map calculated only from CI-treated epiblast cells (Fig. 2a).

579   **Extended Data Fig. 3 | Analysis on epiblast cells from DMSO and CI-treated embryo.**

580   **a,** Heatmap showing the expression pattern of all genes differentially expressed along the

581   trajectory from winning to losing cells in Fig. 2d. **b-c,** Overlap of genes differentially expressed

582   along the trajectory joining winning and losing epiblast cells in CI-treated embryos (Fig. 2a and

583   panel d) and genes targeted by p53. Pie charts show the percentage of genes up- or down-

584   regulated in loser cells within the group of target genes that are activated (**b**) or repressed (**c**) by

585   p53. There is an enrichment of activated/repressed targets among genes

586   upregulated/downregulated in losing cells respectively (Fisher's test, p-value=1E-4). The list of

587   p53 targets is taken from[59]. **d,** Scatter plots of the expression levels of different marker genes

588   plotted against each other in loser epiblast cells (cluster 4). Loser cells have higher expression

589   of pluripotency markers as well as higher expression of some lineage-specific markers and the

590   co-expression of these markers is only weakly correlated. **e-g** Our scRNA-seq data from epiblast

591   cells is projected on top of previously published data from epiblast collected from freshly isolated

592   embryos at different stages (E5.5, E6.25 and E6.5; data from[26]). First, a diffusion map (**e**) and a

593   pseudotime coordinate (**f**) is computed for the epiblast cells from freshly isolated embryos. Then,

594   a pseudotime coordinate is estimated for our data after projecting it onto the diffusion map.

595   Panel **g** shows the pseudotime coordinates for both datasets, split by stage, treatment and

596   cluster.

597   **Extended Data Fig. 4 | Cells eliminated during early mouse embryogenesis have activated**

598   **stress responses.**

599   **a**, Overlap of genes differentially expressed along the trajectory joining winning and losing

600   epiblast cells in CI-treated embryos (Fig. 2a and Extended Data Fig. 3a) and genes related to

601   the unfolded protein response and integrated protein response pathways (UPR_ISR, see

602   Supplementary Table 3). From the 32 genes related to the UPR & ISR pathways, 12 are down-

603   regulated in loser cells, 8 genes are up-regulated in loser cells, and 12 genes are not

26

604   differently expressed between loser and winner cells. There is a statistically significant

605   enrichment of UPR&ISR genes among the up-regulated genes in loser cells (Fisher test, odds

606   ratio=3.0, p-value=0.012). The intersection between UPR-ISR genes and the down regulated

607   genes is not significant (Fisher test, odds ratio=1.2, p value=0.69). **b-c,** List of genes from UPR-

608   ISR pathways that are statistically significantly up-regulated (**b**) or down-regulated (**c**) in loser

609   cells. **d,** Scatterplots with the expression levels of genes involved in stress responses in epiblast

610   cells from CI-treated embryos as a function of cells' losing score. **e,** Experimental design with the

611   approach taken to validate the expression of the stress response marker DDIT3 in epiblast cells

612   from DMSO or CI-treated embryos. **f,** Representative micrographs of DMSO (upper panel) or CI-

613   treated embryos (100 µM, lower panel) stained for DDIT3, quantified in (**g**). Nuclei are labelled

614   with Hoechst. In control embryos (DMSO-treated), dying cells in the cavity show very high

615   DDIT3 expression (arrow), while live cells in the epiblast of the CI-treated embryos show more

616   modest levels of DDIT3 expression (arrowheads). Scale bar = 20 µm. **g,** Quantification of the

617   percentage of epiblast cells with nuclear DDIT3 expression. N=10 DMSO and N=9 CI-treated

618   embryos. Data shown as mean ± SEM. *Ddit3 (Chop)*, DNA-damage inducible transcript 3; *Atf3*,

619   activating transcription factor 3; *Atf4*, activating transcription factor 4; *Foxo3*, forkhead box O3;

620   *Ppp1r115a (Gadd34),* Protein Phosphatase 1 Regulatory Subunit 15A, *Eif2ak3 (Perk),*

621   Eukaryotic Translation Initiation Factor 2 Alpha Kinase 3; *Nfe2l2 (Nrf2)*, NFE2-related factor 2;.

622   *Sesn2*, Sestrin 2; *Gdf15*, Growth Differentiation Factor 15; *Mthfd1l*, Methylenetetrahydrofolate

623   Dehydrogenase (NADP$^+$ Dependent) 1 Like; *Hspe1*, Heat Shock Protein Family E (*Hsp10*)

624   Member 1; *Cat*, Catalase; *Hspd1*, Heat Shock Protein Family D (Hsp60) Member 1; *Sod2,*

625   Superoxide Dismutase 2; *Hsph1,* Heat Shock Protein Family H (*Hsp110*) Member 1; *Lonp1*, Lon

626   Peptidase 1, Mitochondrial; *Eif2a,* Eukaryotic Translation Initiation Factor 2A; *Mthfd2*,

627   Methylenetetrahydrofolate Dehydrogenase (NADP$^+$ Dependent) 2, Methenyltetrahydrofolate

628   Cyclohydrolase; *Hspa4*, Heat Shock Protein Family A (*Hsp70*) Member 4; *Cth*, Cystathionine

629   Gamma-Lyase; *Nrf1*, Nuclear Factor 1.

630   **Extended Data Fig. 5 | Mitochondrial function in Wild-type, *Bmpr1a*$^{-/-}$ and 4n mESCs.**

631   **a-d,** Metabolic flux analysis of wild-type and *Bmpr1a*^{-/-} mESCs. OCR profile and metabolic

632   parameters assessed during the mitochondria stress test performed in pluripotency conditions

633   (**a**). ECAR profile and metabolic parameters assessed during the glycolysis stress test

634   performed in pluripotency conditions (**b**). Metabolic parameters from the mitochondria stress test

635   found to be similar between wild-type and *Bmpr1a*^{-/-} mESCs during differentiation – day 3 (**c**).

636   Metabolic parameters from the glycolysis stress test found to be similar between wild-type and

637   *Bmpr1a*^{-/-} mESCs during differentiation – day 3 (**d**). Data obtained with a minimum of 3

638   independent experiments, with 5 replicates per cell type in each assay. Statistical analysis done

639   with Mann-Whitney test. **e-f,** Analysis of mitochondrial membrane potential ($\Delta\psi$m) in defective

640   mESCs maintained in pluripotency conditions, in separate or co-culture. Representative

641   histograms of TMRM fluorescence and quantification for wild-type and *Bmpr1a*^{-/-} (**e**) and wild-

642   type and 4n (**f**). Statistical analysis done by two-way ANOVA, followed by Holm-Sidak's multiple

643   comparisons test. **g,** Analysis of mitochondrial ROS in wild-type and *Bmpr1a*^{-/-} mESCs

644   undergoing differentiation in separate or co-culture: representative histograms of mitoSOX Red

645   fluorescence and quantification of the percentage of mitoSOX positive cells. Statistical analysis

646   done by two-way ANOVA, followed by Holm-Sidak's multiple comparisons test. Data obtained

647   with a minimum of 3 independent experiments. Error bars represent SEM.

648   **Extended Data Fig. 6 | Effect of actinonin in OPA1 expression in wild-type and *Drp1*^{-/-}**

649   **cells. a**, Western blot analysis of OPA1 expression in wild-type and *Drp1*^{-/-} cells treated with

650   actinonin (Act, 150 µM) during 6 hours on the third day of differentiation, quantified in (**b-c**). **b-c**,

651   Expression levels of L-OPA1 (**b**) and S-OPA1 (**c**) relative to α-tubulin. Data shown as mean ±

652   SEM of a minimum of 3 independent experiments. Statistical analysis done by two-way ANOVA,

653   followed by Holm-Sidak's multiple comparisons test.

654   **Extended Data Fig. 7 | Analysis of SNPs in mtDNA in epiblast cells.**

655   **a-e,** mtDNA heteroplasmy in epiblast cells from CI-treated embryos for five positions within the

656   *mt-Rnr2* gene. All of these positions have an heteroplasmy that increases with the cells' losing

657   scores in a statistically significant way (the adjusted p-value estimated via a generalized linear

28

658 model is indicated at the top of each plot). **f-k,** The variation in the heteroplasmy across the CI-

659 treated cells is not due to a batch effect for the 6 significant positions within the *mt-Rnr1* gene. **l,**

660 Spearman's correlation between the mtDNA heteroplasmy at all the statistically significant

661 positions (six within the gene mt-*Rnr1* and five within the gene mt-*Rnr2*).

662 **Extended Data Fig. 8 | Changes in mtDNA sequence are enough to trigger cell**

663 **competition.**

664 **a**, Illustration of the process of derivation of the mESCs lines from mice that are hybrid between

665 the wild-caught strains (BG, HB or ST) and the lab mouse (C57BL/6N). These hybrid mice were

666 generated elsewhere[16] by ooplasmic transfer: the zygote of a C57BL/6N mouse was injected

667 with ooplasm from a wild-caught mouse (orange, HB pictured). Therefore, these hybrid mice

668 contain the nuclear background of the C57BL/6N strain and the mtDNA of wild-caught strain and

669 potentially C57BL/6N mtDNA (heteroplasmic mice strains). mESCs lines were derived from the

670 hybrid mice and characterised. **b-f,** Characterisation of the derived cell lines by flow cytometry,

671 during pluripotency, in comparison to the wild-type cell line used in previous experiments (E14,

672 129/Ola background). Heteroplasmy analysis of the derived mESC lines from the hybrid mice,

673 indicating the percentage of wild-derived mtDNA (**b**). Cell granularity (internal complexity) given

674 as median fluorescence intensity of SSc-A laser (**c**). Cell size given as median fluorescence

675 intensity of FSc-A laser (**d**). Analysis of the expression of mitochondrial markers: representative

676 western blot and quantification of markers of mitochondrial mass (ATPB, mt-CO1 and TOMM20)

677 and mitochondrial dynamics (DRP1, MFN1and MFN2), relative to vinculin, in cells derived from

678 hybrid mice (**e**). **f,** Representative histograms and quantification of median TMRM fluorescence,

679 indicative of Δψm, for the hybrid cell lines derived, in comparison to the wild-type cell line used in

680 previous experiments (E14, 129/Ola background). Statistical analysis done by one-way ANOVA,

681 followed by Holm-Sidak's multiple comparisons test. **g-i,** Cell competition assays between hybrid

682 cell lines maintained in pluripotency culture conditions. The ratio of final/initial cell numbers in

683 separate or co-culture is shown. Statistical analysis done by two-way ANOVA, followed by Holm-

684 Sidak's multiple comparisons test. **j,** Experimental design for RNA-Seq and gene set enrichment

29

685   analysis (GSEA). The isolation of RNA from winner HB(24%) and loser BG(95%) cells was

686   performed after three days in separate or co-culture conditions, once cells have been subjected

687   to FACS to isolate the two populations form mixed cultures. Data obtained with a minimum of 3

688   independent experiments. Error bars represent SEM.

689   **Extended Data Fig. 9 | Metabolic flux analysis of the cells with different mtDNA variants:**

690   **HB(100%), HB(24%), BG(95%) and C57BL/6N. a,** OCR profile during mitochondria stress test

691   performed in pluripotency maintenance conditions. **b-i,** Metabolic parameters assessed during

692   the during the mitochondria stress test performed in pluripotency conditions. Data obtained with

693   a minimum of 3 independent experiments, with 5 replicates per cell type in each assay. Error

694   bars represent SEM. Statistical analysis done with Kruskal-Wallis test, followed by Dunn's

695   multiple comparison test.

696   **Extended Data Fig. 10 | Common features of scRNA-seq and bulk RNA-seq datasets.**

697   **a,** Terms significantly enriched among genes downregulated in BG(95%) (loser) ESCs *in vitro*

698   when co-cultured with HB(24%) cells. The loss of mitochondrial activity emerges as a common

699   feature between loser cells *in vivo* and *in vitro*. The gene enrichment analysis was performed

700   using g-profiler tool (see Methods). **b,** Intersection between differentially expressed genes along

701   the trajectory from winning to losing epiblast cells ("in_vivo_scRNA-seq"; Fig. 2a and Extended

702   Data Fig. 3a and genes differentially expressed between co-cultured HB(24%) (winner) and

703   BG(95%) (loser) ESCs ("in_vitro_bulk_RNA-seq"). "Up" and "Down" here refer to genes up- or

704   down-regulated in loser cells. Fisher test for the intersection between down-regulated genes

705   from scRNA-seq (*in vivo*) and down-regulated genes from bulk RNA-seq (*in vitro*): p-value,

706   1.71E-12; odds ratio 1.80. Fisher test for the intersection between down-regulated genes from

707   scRNA-seq (*in vivo*) and up-regulated genes from bulk RNA-seq (*in vitro*): p-value, 5.20E-3;

708   odds ratio 0.67**.** Fisher test for the intersection between up-regulated genes from scRNA-seq (*in*

709   *vivo*) and down-regulated genes from bulk RNA-seq (*in vitro*): Fisher test p-value, 4.87E-3; odds

710   ratio 0.80. The intersection between up-regulated genes from sc-RNA-seq (*in vivo*) and up-

711   regulated genes from bulk RNA-Seq (*in vitro*) is not statistically significant: Fisher test p-value:

712   0.30, odds ratio 1.14. **c,** Intersection between the significantly enriched terms in genes

713   upregulated or downregulated in loser cells in the epiblast of CI-treated embryos

714   ("*in_vivo*_scRNA-Seq") or in our *in vitro* model of competition between co-cultured HB(24%)

715   (winner) and BG(95%) (loser) ESCs ("*in_vitro*_bulk_RNA-seq"). All the terms enriched among

716   downregulated genes *in vitro* are also enriched *in vivo*.

List of Tables.

718   **Supplementary Table 1.** List of genes down-regulated along the winner-to-loser trajectory in the

719   embryo.

720   **Supplementary Table 2.** List of genes up-regulated along the winner-to-loser trajectory in the

721   embryo.

722   **Supplementary Table 3.** Genes related to the unfolded protein response and integrated protein

723   response pathways (UPR_ISR) that were analysed in the genes differentially expressed along

724   the winner-to-loser trajectory.

725   **Supplementary Table 4.** List of background genes for the winner-to-loser trajectory in the

726   embryo.

727   **Supplementary Table 5.** List of genes down-regulated in BG(95%) cells when co-cultured with

728   HB(24%) cells.

729   **Supplementary Table 6.** List of genes up-regulated in BG(95%) cells when co-cultured with

730   HB(24%) cells.

731   **Supplementary Table 7.** List of background genes used for the analysis of genes differentially

732   expressed between co-cultured BG(95%) and HB(24%) cells.

31

Methods

733

Animals

734

735 Mice were maintained and treated in accordance with the Home Office's Animals (Scientific

736 Procedures) Act 1986 and covered by the Home Office project license PBBEBDCDA. All mice

737 were housed on a 10 hr-14 hr light-dark cycle with access to water and food *ad libitum*. Mattings

738 were generally set up in the afternoon. Noon of the day of finding a vaginal plug was designated

739 embryonic day 0.5 (E0.5). Embryo dissection was performed at appropriate timepoints in M2

740 media (Sigma), using Dumont No.5 forceps (11251-10, FST). No distinction was made between

741 male and female embryos during the analysis.

Cell lines, cell culture routine and drug treatments

742

743 E14, kindly provided by Prof A. Smith, from Cambridge University, were used as wild-type

744 control cells tdTomato-labelled or unlabelled. GFP-labelled or unlabelled cells defective for BMP

745 signalling (*Bmpr1a$^{-/-}$*), tetraploid cells (4n) and *Bmp1a$^{-/-}$* null for p53 *(Bmpr1a$^{-/-}$;p53$^{/-}$)* are

746 described elsewhere [6, 7]. Cells null for Dynamin-related protein 1 (*Drp1$^{-/-}$*) or Mitofusin 2 (*Mfn2$^{-/-}$*)

747 were generated by CRISPR mutagenesis. Cells with different mitochondrial DNA (mtDNA)

748 content in the same nuclear background were derived from embryos of hybrid mice, generated

749 elsewhere [16].

750 Cells were maintained pluripotent and cultured at 37ºC in 5% CO_2 in 25 cm^2 flasks (Nunc)

751 coated with 0.1% gelatin (Sigma) in DPBS. Growth media (ES media) consisted of GMEM

752 supplemented with 10% FCS, 1 mM sodium pyruvate, 2 mM L-glutamine, 1X minimum essential

753 media non-essential amino-acids, 0.1 mM β-mercaptoethanol (all from Gibco) and 0.1%

754 leukemia inhibitory factor (LIF, produced and tested in the lab). Cells derived from hybrid mice

755 (C57BL/6N nuclear background) were maintained on 0.2% LIF. The growth media was changed

756 daily, and cells were split every 3 days.

757 To manipulate mitochondrial translation during differentiation, wild-type and *Drp1$^{-/-}$* mESCs were

758 treated with doxycycline (Dox, 22.5 µM), from day 1 to day 3 of culture, or with actinonin (Act,

32

759   150 µM), for 6 hours on day 3 of culture in N2B27 media (see Differentiation and Cell

760   competition assays). As control condition, cells were treated with vehicle (Con). Samples were

761   collected on day 3 of differentiation for western blot analysis.

762

763   **CRISPR mutagenesis**

764   Drp1 and Mfn2 knockout ESCs were generated by CRISPR-Cas9 mediated deletion of Drp1

765   exon 2 and Mfn2 exon 3 respectively. sgRNA guides flanking Drp1 exon 2 or Mfn2 exon 3 were

766   cloned into the PX459 vector (Addgene)[60]: Drp1 exon 2 upstream sgRNA:

767   5' TGGAACGGTCACAGCTGCAC 3'; Drp1 exon 2 downstream sgRNA:

768   5' TGGTCGCTGAGTTTGAGGCC 3'; Mfn2 upstream sgRNA: 5' GTGGTATGACCAATCCCAGA

769   3'; Mfn2 downstream sgRNA: 5' GGCCGGCCACTCTGCACCTT 3'. E14 ESCs were co-

770   transfected with 1ug of each sgRNA expression using Lipofectamine 2000 (Invitrogen) according

771   to manufacturer's instructions. As control E14 ESCs were transfected in parallel with equal

772   amount of empty PX459 plasmid. Following 6 days of Puromycin selection, single colonies were

773   picked from both Drp1 sgRNA and empty vector transfected ESCs and screened for

774   mutations. Drp1 exon 2 deletion was confirmed by PCR genotyping using the following primers:

775   Drp1_genot F: 5' GGATACCCCAAGATTTCTGGA 3'; Drp1_genot R: 5'

776   AGTCAGGTAATCGGGAGGAAA 3', followed by Sanger Sequencing. Mfn2 exon 3 deletion was

777   confirmed by PCR genotyping using the following primers: Mfn2_genot F: 5'

778   CAGCCCAGACATTGTTGCTTA 3'; Mfn2_genot R: 5' AGCTGCCTCTCAGGAAATGAG 3',

779   followed by Sanger Sequencing.

780   **Derivation of mESCs from hybrid mouse strains and heteroplasmy determination**

781   The derivation of new mESC lines was adapted from [61]. Cells were derived from embryos of

782   hybrid mouse strains BG, HB and ST. These contain the mtDNA of C57BL/6N (Bl6) lab mouse

783   and mtDNA variants from wild-caught mice [16].

784　Embryos were isolated at E2.5 (morula stage) and cultured in 4-well plates (Nunc, Thermo

785　Scientific) containing KSOM media (Millipore) plus two inhibitors (KSOM+2i): 1 μM MEK inhibitor

786　PDO325901 (Sigma-Aldrich) and 3 μM GSK-3 inhibitor CHIR9902 (Cayman Chemicals) for 2

787　days at 37ºC in 5% CO_2 incubator. To reduce evaporation, the area surrounding the wells was

788　filled with DPBS. Embryos were further cultured in a fresh 4-well plates containing,

789　N2B27+2i+LIF media: N2B27 media supplemented with 1 μM MEK inhibitor PDO325901 and 3

790　μM GSK-3 inhibitor and 0.1% LIF for up to 3 days until reaching the blastocyst stage. Each

791　embryo was then transferred to a well of a 96-well plate coated with 0.1% gelatin in DPBS and

792　containing 150 μL of N2B27+2i+LIF media per well. In these conditions, the embryos should

793　attach to the wells allowing the epiblast to form an outgrowth. This plate was then incubated at

794　37ºC in 5% CO_2 incubator for 3 to 7 days until ES-like colonies start to develop from the epiblast

795　outgrowth. Cells were passaged by dissociation with Accutase (Sigma) and seeded in gradual

796　increasing surface area of growth (48-well, 24-well, 12-well plate, T12.5 and T25 flask), until new

797　cell lines were established. At this stage cells were weaned from N2B27+2i+LIF media and then

798　routinely cultured in ES media.

799　These new cell lines were then subjected to characterisation by flow cytometry (cell size,

800　granularity and mitochondrial membrane potential) and ARMS-qPCR assay[16] (to determine

801　heteroplasmy).

802　**Embryo experiments**

803　Early mouse embryos were isolated at E5.5 (from pregnant CD1 females, purchased from

804　Charles River, UK). Following dissection from the decidua, embryos were cultured overnight in

805　N2B27 "poor" media (same formulation as N2B27 media but supplemented with 0.5xB27

806　supplement and 0.5xN2 supplement) with pan-caspase inhibitors (100 μM, Z-VAD-FMK,

807　FMK001, R&D Systems, USA) or equal volume of vehicle (DMSO) as control. On the next

808　morning, embryos were processed for single cell RNA-Seq (scRNA-seq) or functional validation

809　(Δψm analysis and immunohistochemistry for markers of loser cells).

34

810   For the scRNA-seq and Δψm analysis embryos were dissociated into singe-cells. Briefly, up to

811   12 embryos were dissociated in 600 µL Acccutase (A6964, Sigma, UK) during 12 min at 37ºC,

812   tapping the tube every two minutes. Accutase was then neutralised with equal volume of FCS,

813   cells span down and stained with TMRM, for Δψm analysis, or directly re-suspended in 300 µL

814   DPBS with 1% FCS, for single cell sorting and RNA-seq. Sytox blue (1:1000, S34857,

815   ThermoFisher Scientific, UK), was used as viability staining.

816   **Differentiation and Cell competition assays**

817   Cell competition assays between wild-type and *Bmpr1a*^{-/-}, 4n or *Drp1*^{-/-} cells were performed in

818   differentiating conditions. Cells were seeded onto fibronectin-coated plates (1:100, Merck) in

819   DPBS during 1h at 37ºC and grown in N2B27 media - to promote the differentiation of mESCs

820   into a stage resembling the post-implantation epiblast, as cell competition was previously shown

821   to occur in these conditions [6]. N2B27 media consisted of 1:1 Dulbecco's modified eagle medium

822   nutrient mixture (DMEM/F12) and Neurobasal supplemented with N2 (1x) and B27 (1x)

823   supplements, 2 mM L-glutamine and 0.1 mM β-mercaptoethanol - all from Gibco. Cell

824   competition assays between wild-type and *Mfn2*^{-/-} and between mESCs with different mtDNA

825   content were performed in pluripotency maintenance conditions (ES media).

826   Cells were seeded either separately or mixed for co-cultures at a 50:50 ratio, onto 12 well plates,

827   at a density of 8E04 cells per well, except for assays between wild-type and *Mfn2*^{-/-} mESCs,

828   where 3.2E05 cells were seeded per well. The growth of cells was followed daily and compared

829   between separate or co-culture, to control for cell intrinsic growth differences, until the fourth day

830   of culture. Viable cells were counted daily using Vi-CELL XR Analyser (Beckman Coulter, USA),

831   and proportions of each cell type in co-cultures were determined using LSR II Flow Cytometer

832   (BD Bioscience), based on the fluorescent tag of the ubiquitously expressed GFP or TdTomato

833   in one of the cell populations.

834   **Metabolomic analysis**

835   The metabolic profile was obtained using the Metabolon Platform (Metabolon, Inc). Each sample

836   consisted of 5 biological replicates. For each replicate, 1E07 cells were spun down and snap

837   frozen in liquid nitrogen. Pellets from 5 independent experiments for each condition were

838   analysed by Metabolon Inc by a combination of Ultrahigh Performance Liquid Chromatography-

839   Tandem Mass Spectroscopy (UPLC- MS/MS) and Gas Chromatography-Mass Spectroscopy

840   (GC-MS). Compounds were identified by comparison to library entries of purified standards

841   based on the retention time/index (RI), mass to charge ratio (m/z), and chromatographic data

842   (including MS/MS spectral data) on all molecules present in the library. Samples were

843   normalized to protein content measured by Bradford assay. Statistical analysis was done using

844   Welch's two-sample t-test and statistical significance defined as $p \leq 0.05$.

845   **Seahorse analysis**

846   The metabolic function of cells was assessed by extracellular flux analysis using Seahorse XF24

847   (Agilent Technologies, UK). For assays ran during pluripotency, cells were seeded, on the day

848   prior to the assay, onto 0.1% gelatin-coated (Sigma, UK) in 300 µL of ES media. All cell types

849   were seeded at 5×10^4 cells per well, except for $Bmpr1a^{-/-}$ cells, that were seeded at 6E04 per

850   well). For assays ran during differentiation, cells were seeded, the 3 days before the assay, onto

851   fibronectin-coated fibronectin-coated plates (1:100, Merck, UK), in 300 µL of N2B27media. All

852   cell types were seeded at 2.4E04 cells per well, except for $Bmpr1a^{-/-}$ cells, that were seeded at

853   3.2E04 cells per well.

854   On the day of the assay, cells were carefully washed twice with assay media and then left with a

855   final volume of the 600 µL per well. The plate was then equilibrated on a non-CO_2 incubator at

856   37ºC for 30 min. The assay media consisted in unbuffered DMEM (D5030 – Sigma, UK), that

857   was supplemented on the day of the assay according to the test performed. For the OCR

858   measurements the assay media was supplemented with 0.5 g.L−1 of glucose (Sigma, UK) and 2

859   mM of L-glutamine (Life Technologies, UK), while for the ECAR measurements the media was

860   supplemented with 1 mM of Sodium Pyruvate and 2 mM of L-glutamine (both from Life

861   Technologies, UK), pH 7.4 at 37ºC.

862 The protocol for the assay consisted of 4 baseline measurements and 3 measurements after

863 each compound addition. Compounds (all from Sigma, UK) used in OCR and ECAR assays

864 were prepared in the supplemented assay media. For the OCR assay, test the following

865 compounds were added: 1 mM Pyruvate (Pyr), 2.5 μM oligomycin (OM), 300 nM Carbonyl

866 cyanide-4-(trifluoromethoxy) phenylhydrazone (FCCP) and a mixture of rotenone and antimycin

867 A at 6 μM each (R&A). For the ECAR assay, the following compounds were added: 2.5 mM and

868 10 mM of glucose, 2.5 μM of oligomycin (OM), and a 50 mM of 2-deoxyglucose (2-DG).

869 Each of the experiments was performed in 3 times, with 5 biological replicates of each cell type.

870 For background correction measurements, 4 wells were left without cells (A1, B4, C3 and D6).

871 Both ECAR and OCR measurements were performed on the same plate. The assay parameters

872 for both tests were calculated following the Seahorse assay report generator (Agilent

873 Technologies, UK).

874 At the end of the assay, cells were fixed and stained with Hoechst. Both OCR and ECAR were

875 normalised to cell number, determined by manual cell counts using Fiji software. The

876 normalisation of the data was processed on Wave Desktop software (Agilent Technologies, UK)

877 and data exported to Prism 8 (GraphPad) for statistical analysis.

878 **Analysis of mitochondrial membrane potential (Δψm) and mitochondrial ROS**

879 Quantitative analysis of Δψm and mitochondrial ROS was performed by flow cytometry. Cells

880 were grown in pluripotency or differentiating conditions, as described above. Cells were

881 dissociated and pelleted to obtain 2E05 cells per sample for the staining procedure.

882 For TMRM staining in single cells from early mouse epiblasts, embryos were dissected at E5.5

883 and cultured overnight in the presence or absence of caspase inhibitors. On the following

884 morning, to avoid misleading readings, epiblasts were isolated initially by an enzymatic

885 treatment with of 2.5% pancreatin, 0.5% trypsin and 0.5% polyvinylpyrrolidone (PVP40) - all from

886 Sigma-Aldrich- to remove the visceral endoderm (VE). Embryos were treated during 8 min at

887 4ºC, followed by 2 min at RT. The VE was then pealed with the forceps and the extraembryonic

888 ectoderm removed to isolate the epiblasts. Up to 16 epiblasts were pooled per 600μL of

37

889   Accutase (Sigma-Aldrich) for dissociation into single cells prior to staining. Reaction was

890   stopped with equal volume of FCS and cells subjected to TMRM staining.

891   Cells were loaded with 10 nM of the Nernstian probe tetramethylrhodamin methyl ester

892   perchlorate (TMRM, Sigma), prepared in N2B27 media. After incubating for 15 min at 37ºC, cells

893   were pelleted again and re-suspended in flow cytometry (FC) buffer (3% FCS in DPBS). Sytox

894   blue (1:1000, Invitrogen, UK) was used as viability staining. Stained cell suspensions were

895   analysed in BD LSRII flow cytometer operated through FACSDiva software (Becton Dickinson

896   Biosciences, UK). For TMRM fluorescence detection the yellow laser was adjusted for excitation

897   at λ=562 nm, capturing the emission light at λ=585 nm for TMRM. In the case of GFP-labelled

898   cell lines, for GFP fluorescence detection the blue laser was adjusted for excitation at λ=488 nm,

899   capturing the emission light at λ=525 nm. Results were analysed in FlowJo vX10.0.7r2.

900   Qualitative analysis of Δψm was performed by confocal microscopy. Wild-type and $Bmpr1a^{-/-}$

901   cells were grown in fibronectin-coated glass coverslips. On the third day of differentiation, cells

902   were loaded with 200 nM MitoTracker Red probe (Life Technologies), prepared in N2B27 media,

903   for 15 min at 37ºC. Cells were then washed with DPBS and fixed with 3.7% formaldehyde for

904   subsequent immunocytochemical staining of total mitochondria mass, with TOMM20 antibody.

905   For the analysis of mitochondrial ROS, cells were grown in differentiating conditions and stained

906   on the third day of culture. Briefly, 2E05 cells of each cell line were resuspended in 200 μL of 5

907   μM solution of MitoSOX (Invitrogen, UK) prepared in N2B27 media. Cells were incubated at

908   37ºC for 15 min, and then resuspended in FC buffer. MitoSOX fluorescence was analysed with

909   the violet laser adjusted for excitation at λ=405 nm, capturing the emission light at λ=610 nm.

910   Sytox blue was used as viability staining.

911   **Immunofluorescence**

912   Cells were washed with DPBS and fixed with 3.7% formaldehyde (Sigma, UK) in N2B27, for 15

913   min at 37ºC. Permeabilization of the cell membranes was done with 0.4% Triton X-100 in DPBS

914   (DPBS-Tx), at RT with agitation. Blocking step with 5% BSA in DPBS-Tx 0.1% was performed

915   for 30 min, at RT with agitation. Mitochondria were labelled with TOMM20 antibody (1:100,

38

916   Santa Cruz Biotechnologies). Dead cells were labelled with cleaved caspase-3 antibody (1:400,

917   CST) and NANOG antibody was used to mark pluripotent cells (1:100, eBioscience). Secondary

918   antibodies were Alexa Fluor (1:600, Invitrogen). Primary antibody incubation was performed

919   overnight at 4ºC and secondary antibody incubation during 45 min, together with Hoechst to

920   stain nuclei (1:1000, ThermoScientific), at RT and protected from light. In both cases antibodies

921   were diluted in blocking solution. Three 10 min washes with DPBS-Tx 0.1% were performed

922   between each critical step and before mounting with Vectashield medium (Vector Laboratories).

923   Samples were imaged with a Zeiss LSM780 confocal microscope (Zeiss, UK) and processed

924   with Fiji software [62]. Mitochondria stainings were imaged with a 63x/1.4 Oil objective. For

925   samples stained with TOMM20 antibody and MitoTracker Red, Z-stacks were acquired and

926   processed for deconvolution using Huygens software (Scientific Volume Imaging, https://svi.nl/).

927   Samples stained with cleaved caspase-3 were imaged with 20x/0.8 air objective. Imaging and

928   deconvolution analysis were performed with the support and advice from Mr. Stephen Rothery

929   from the Facility for Imaging by Light Microscopy (FILM) at Imperial College London.

930   Embryo immunofluorescent staining for p-rpS6, OPA1 and DDIT3 (CHOP) markers was

931   performed as follows. Cultured embryos were fixed in 4% PFA in DPBS containing 0.01% Triton

932   and 0.1% Tween 20 during 20 min at RT. Permeabilization of the membranes was done during

933   10 min in DPBS with 0.5% Triton. Embryos were blocked in 5% BSA in DPBS with 0.25% Triton

934   during 45 min. Incubation with primary antibodies - CHOP (1:500, CST- 2895S), OPA1 (1:100,

935   BD Biosciences - 612606) and p-rpS6 (CST - 5364) - was done overnight at 4ºC in 2.5% BSA in

936   DPBS with 0.125% Triton. On the following morning, hybridisation with secondary antibodies

937   Alexa Fluor 568 and Alexa Fluor 488 (diluted 1:600 in DPBS with 2.5% BSA and 0.125% Triton)

938   was done next during 1h at RT. Hoechst was also added to this mixture to stain nuclei (1:1000,

939   Invitrogen). Three 10 min washes with filtered DPBS-Tx 0.1% were performed between each

940   critical step. All steps were done with gentle agitation.

941   Embryos were imaged in embryo dishes (Nunc) in a drop of Vectashield using Zeiss LSM780

942   confocal microscope at 40x/1.3 oil objective.

39

943   Further details about image acquisition and processing are specified in the Supplementary

944   Methods file "Imaging equipment and settings.docx"

945   **Western Blotting**

946   Cells were washed in DPBS and lysed with Laemmli lysis buffer (0.05 M Tris- HCl at pH 6.8, 1%

947   SDS, 10% glycerol, 0.1% β-mercaptoethanol in distilled water). Total protein quantification was

948   done using BCA assay (Thermo Scientific, UK) and samples (15µg of protein per lane) were

949   loaded into 12% Bis-Tris protein gels (BioRad). Resolved proteins were transferred into

950   nitrocellulose membranes (GE Healthcare). The following primary antibodies were incubated

951   overnight at 4ºC: rabbit anti-TOMM20 (1:1000, CST - 42406), rabbit anti-α-Tubulin (1:1000,

952   CST- 2144), mouse anti-mt-CO1 (1:2000, Abcam - 14705), rabbit anti-DRP1 (1:1000, CST-

953   8570), mouse anti-MFN1 (1:1000, Abcam - 57602), mouse anti-MFN2 (1:500, Abcam - 56889),

954   mouse anti-Vinculin (1:1000, Sigma - V9131), mouse anti-OPA1 (1:1000, BD Biosciences -

955   612606), rabbit anti-ATF4 (1:1000, CST-11815), rabbit anti-α-PCNA (1:1000, Abcam - 2426)

956   and rabbit anti-p-eIF2α (Ser51, 1:1000, CST-9721). On the following morning, HRP-conjugated

957   secondary antibodies (Santa Cruz) were incubated for 1h at RT. Membranes were developed

958   with ECL reagents (Promega) and mounted in cassette for time-time-controlled exposure to film

959   (GE Healthcare).

960   **Bulk RNA-Seq and Single cell RNA-Seq**

961   For bulk RNA Seq in the competitive scenario between cells with different mtDNA, HB(24%) and

962   BG(95%) mESCs were grown separately or in co-culture. On the third day of culture cells were

963   dissociated and subjected to fluorescence activated cell sorting (FACS) to separate the cell

964   populations in co-culture. To control for eventual transcriptional changes due to the FACS

965   process, a mixture of the two separate populations was subjected to the same procedure as the

966   co-cultured samples. Total RNA isolation was then carried out using RNA extraction Kit (RNeasy

967   Mini Kit, Qiagen). PolyA selection/enrichment was the method adopted for library preparation,

968   using the NEB Ultra II RNA Prep Kit. Single end 50bp libraries were sequenced on Illumina

969   Hiseq 2500. Raw basecall files were converted to fastq files using Illumina's bcl2fastq (version

40

970   2.1.7). Reads were aligned to the mouse genome (mm9) using Tophat2 version 2.0.11 [63] with

971   default parameters. Mapped reads that fell on genes were counted using featureCounts from

972   Rsubread package [64]. Generated count data were then used to identify differentially expressed

973   genes using DESeq2 [65]. Genes with very low read counts were excluded. Finally, Gene Set

974   Enrichment Analysis was performed using GSEA software [66, 67] on pre-ranked list generated by

975   DESeq2.

976   To investigate the nature of cells eliminated by cell competition during early mouse

977   embryogenesis by means of Single Cell RNA-Sequencing (scRNA-seq), early mouse embryos

978   were dissected at E5.5 and cultured overnight in the presence or absence of caspase inhibitors.

979   On the following morning, embryos were dissociated with Accutase and subjected to single-cell

980   sorting into 384-well plates. Total RNA isolation was then carried out using a RNA extraction Kit

981   (RNeasy Mini Kit, Qiagen). scRNA-seq was performed using the Smart-seq2 protocol[68]. PolyA

982   selection/enrichment with Ultra II Kit (NEB) was the method adopted for library preparation.

983   **Data processing, quality control and normalization**

984   We performed transcript quantification in our scRNA-seq data by running Salmon v0.8.2 [69] in the

985   quasi-mapping-based mode. First, a transcriptome index was created from the mouse reference

986   (version GRCm38.p4) and ERCC spike-in sequences. Then, the quantification step was carried

987   out with the "quant" function, correcting for the sequence-specific biases ("--seqBias" flag) and

988   the fragment-level GC biases ("--gcBias" flag). Finally, the transcript level abundances were

989   aggregated to gene level counts. On the resulting raw count matrix including 1,495 cells, we

990   apply a quality control to exclude poor quality cells from downstream analyses.

991   For the quality control we used the following criteria: we identified the cells that have a $\log_{10}$ total

992   number of reads equal to or greater than 4, a fraction of mapped reads equal to or greater than

993   0.8, a number of genes with expression level above 10 reads per million equal to or greater than

994   3000 and a fraction of reads mapped to endogenous genes equal to or greater than 0.5. This

995   resulted in the selection of 723 cells, which were kept for downstream analyses. Transcripts per

996   million (TPM) normalization (as estimated by Salmon) was used.

Identification of highly variable genes and dimensionality reduction

To identify highly variable genes (HVG), first we fitted a mean-total variance trend using the R function "trendVar" and then the variance was decomposed into biological and technical components with the R function "decomposeVar"; both functions are included in the package "scran" (version 1.6.9 [70]).

We considered HVGs those that have a biological component that is significantly greater than zero at a false discovery rate (Benjamini-Hochberg method) of 0.05. Then, we applied further filtering steps by keeping only genes that have an average expression greater to or equal than 10 TPM and are significantly correlated with one another (function "correlatePairs" in "scran" package, FDR<0.05). This yielded 1921 genes, which were used to calculate a distance matrix between cells defined as $\sqrt{(1-\rho)/2}$, where ρ is the Spearman's correlation coefficient between cells. A 2D representation of the data was obtained with the UMAP package (version 0.2.0.0 https://cran.r-project.org/web/packages/umap/index.html) using the distance matrix as input.

Cell clustering and connectivity analysis

To classify cells into different clusters, we ran hierarchical clustering on the distance matrix (see above; "hclust" function in R with ward.D2 aggregation method) followed by the dynamic hybrid cut algorithm ("cutreeDynamic" function in R package "dynamicTreeCut" (https://CRAN.R-project.org/package=dynamicTreeCut) version 1.63.1, with the hybrid method, a minimum cluster size of 35 cells and a "deepSplit" parameter equal to 0), which identified five clusters. Cells from different batches were well mixed across these five clusters (see Extended Data Fig. 1), suggesting that the batch effect was negligible. The identity of the five clusters was established based on the expression of known marker genes of Epiblast, Visceral Endoderm and Extra-Embryonic Ectoderm, which were identified in a previous study[56]. The expression levels of some of the top markers is plotted in Figure 1b.

We performed a robustness analysis on the clustering by exploring in detail how the choices of genes, clustering parameters and algorithms affect the identity and the number of clusters. First,

42

1024   we quantified the cluster robustness by calculating Pearson's gamma and the Average

1025   silhouette width obtained with 100 random subsets of 60% of the highly variable genes and

1026   different values of the deepSplit parameter. While the robustness at deepSplit=0 and 1 is similar,

1027   for greater values of deepSplit (corresponding to less conservative clustering) the robustness

1028   rapidly declines (Extended Data Figure 2a). The clustering with deepSplit = 0 and 1 (the more

1029   robust choices) yield very similar results, the only difference being the splitting of the

1030   intermediate cluster in two subclusters (Extended Data Figure 2b).

1031   In addition to this, we also used Louvain clustering on the highly variable genes (resolution=0.3,

1032   k=20 with 20 principal components), which again produced very similar clusters.

1033   We quantified the connectivity between the clusters (using only CI-treated cells) with PAGA[22]

1034   implemented in the python library scanpy (version 1.4.7)[71]. The analysis revealed that the three

1035   epiblast clusters are connected with each other while the two extra embryonic tissues (Visceral

1036   Endoderm and Extra Embryonic Ectoderm) are isolated (Extended Data Figure 2c).

1037   **Identification of a single-cell trajectory in the epiblast**

1038   We calculated a diffusion map ("DiffusionMap" function in the R package "destiny" version 2.6.2

1039   [23] on the distance defined above on the epiblast cells from CI-treated embryos. The pseudotime

1040   coordinate was computed with the "DPT" function with the root cell in the winner epiblast cluster

1041   (identified by the function "tips" in the "destiny" package). Such pseudotime coordinate can be

1042   interpreted as a "losing score" for all the epiblast cells from the CI-treated embryos.

1043   We estimated the losing scores of the epiblast cells from DMSO-treated embryos by projecting

1044   such data onto the diffusion map previously calculated (function "dm_predict" in the destiny

1045   package). Finally, for each of the projected cells, we assigned the losing score as the average of

1046   the losing scores of the 10 closest neighbours in the original diffusion map (detected with the

1047   function "projection-dist" in the destiny package).

1048   While for the clustering and the trajectory analysis we used the highly variable genes computed

1049   from the whole dataset, we verified that all results concerning the separation between winner

1050   and loser epiblast cells (eg, clusters and losing score) remain unaffected if the highly variable

1051   genes are calculated using only the epiblast cells.

1052   **Mapping of data from epiblast cells onto published single-cell RNA seq datasets of**

1053   **epiblast from freshly isolated embryos**

1054   We compared the transcriptional profile of epiblast from embryos cultured in DMSO and CI with

1055   that of epiblast collected from freshly isolated embryos at different stages.

1056   To do this, we considered the dataset published in[26], which includes epiblast cells from embryos

1057   at the stages E5.5 (102 cells), E6.25 (130 cells) and E6.5 (288 cells). A diffusion map and a

1058   diffusion pseudotime coordinate were computed with these cells following the same procedure

1059   described in the section above (Extended Data Figure 2d-e). Then, we projected epiblast cells

1060   from CI and DMSO-treated embryos and we assigned to them a diffusion pseudotime coordinate

1061   as described above (Extended Data Figure 2f).

1062   **Differential gene expression analysis along the trajectory**

1063   To identify the genes that are differentially expressed along the trajectory, first we kept only

1064   genes that have more than 15 TPM in more than 10 cells (this list of genes is provided in

1065   Supplementary Table 4); then, we obtained the log-transformed expression levels of these

1066   genes (adding 1 as a pseudo-count to avoid infinities) as a function of the losing score and we

1067   fitted a generalized additive model to them (R function "gam" from "GAM" package version

1068   1.16.). We used the ANOVA test for parametric effect provided by the gam function to estimate a

1069   p-value for each tested gene. This yielded a list of 5,311 differentially expressed genes (FDR <

1070   0.01).

1071   Next, we looked for groups of differentially expressed genes that share similar expression

1072   patterns along the trajectory. To this aim, similarly to what we did when clustering cells, we

1073   calculated a correlation-based distance matrix between genes, defined as $\sqrt{(1-\rho)/2},$ where ρ

1074   is the Spearman's correlation coefficient between genes. Hierarchical clustering was then

1075   applied to this matrix (hclust function in R, with ward.D2 method) followed by the dynamic hybrid

1076   cut algorithm (dynamicTreeCut package) to define clusters ("cutreeDynamic" function in R with

1077   the hybrid method and a minimum cluster size of 100 genes and a deepSplit parameter equal to

1078   0). This resulted in the definition of four clusters, three of genes that decrease along the

1079   trajectory (merged together for the GO enrichment and the IPA analysis) and one of increasing

1080   genes (Extended Data Fig. 2d). IPA (QIAGEN Inc., https://www.qiagenbio-

1081   informatics.com/products/ingenuity-pathway-analysis), was run on all genes differentially

1082   expressed (FDR < 0.01) along the trajectory from winner to loser cells (see Fig. 2a-d and Fig.

1083   3a-c), using all the tested genes as a background (see Supplementary Table 4). This software

1084   generated networks, canonical pathways and functional analysis. The list of

1085   decreasing/increasing genes is provided in Supplementary Tables 1 and 2.

1086   **Analysis of Mitochondrial DNA heteroplasmy in single-cell RNA seq dataset**

1087   We used STAR (version 2.7 [72]) to align the transcriptome of the epiblast cells from CI-treated

1088   embryos (274) to the mouse reference genome (mm10). Only reads that uniquely mapped to the

1089   mitochondrial DNA (mtDNA) were considered. From these, we obtained allele counts at each

1090   mtDNA position with a Phred Quality Score greater than 33 using the samtools mpileup function.

1091   Next, we applied filters to remove cells and mtDNA positions with a low coverage. First, we

1092   removed cells with fewer than 2,000 mtDNA positions covered by more than 50 reads. Second,

1093   we removed positions having less than 50 reads in more than 50% of cells in each of the three

1094   epiblast clusters (winner, intermediate and loser). These two filters resulted in 259 cells and

1095   5,192 mtDNA positions (covered by ~700 reads per cell on average) being considered for further

1096   analyses.

1097   Starting from these cells and positions, we applied an additional filter to keep only positions with

1098   a sufficiently high level of heteroplasmy. To this aim, for each position with more than 50 reads

1099   in a cell, we estimated the heteroplasmy as:

$$H = 1 - f_{max}$$

1100   where f_{max} is the frequency of the most common allele. We kept only positions with $H>0.01$ in at

1101   least 10 cells.

1102   Finally, using generalized additive models (see above), we identified the positions whose

1103   heteroplasmy H changes as a function of the cells' losing score in a statistically significant way.

1104   We found a total of eleven significant positions (FDR < 0.001), six of them in the *mt-Rnr1* gene

1105   and five in the *mt-Rnr2* gene. All of these positions have a higher level of heteroplasmy in loser

1106   cells (see Fig. 6b-g and Extended Data Fig. 6f-k). The results remain substantially unaltered if

1107   the Spearman's rank correlation test (in alternative to the generalized additive models) is used.

1108   For the barplot shown in Fig. 6h and the correlation heatmaps in Fig. 6i and Extended Data Fig.

1109   6l, we took into account only cells that covered with more than 50 reads all the significant

1110   positions in the *mt-Rnr1* gene (215 cells, Fig. 6h-6i) or in both the *mt-Rnr1* and *mt-Rnr2* genes

1111   (214 cells, Extended Data Fig. 6l).

1112   As a negative control, we repeated the analysis described above using the ERCC spike-ins

1113   added to each cell. As expected, none of the positions was statistically significant, which

1114   suggested that our procedure is robust against sequence errors introduced during PCR

1115   amplification.

1116   We also performed the mtDNA heteroplasmy analysis in cells from the Visceral Endoderm and

1117   the Extra-Embryonic Ectoderm in both DMSO and CI conditions: none of these cells have a

1118   mtDNA heteroplasmy higher than 0.01 in the 11 significant positions identified within mt-Rnr1

1119   and mt-Rnr2 in loser epiblast cells, and the reference allele is always the most common. This

1120   reinforces the hypothesis that such variants are specific to loser epiblast cells and are not

1121   resulting from contamination.

1122   To test the reliability of our heteroplasmy estimations, we used the RNA-seq data from two of the

1123   mtDNA cell lines (BG and HB, see Figure 7), for which the heteroplasmy was measured also by

1124   ARMS-qPCR. To do so, first we downloaded the fasta files of the two mtDNA cell lines from

1125   https://www.ncbi.nlm.nih.gov/nuccore/KC663619.1 and

1126   https://www.ncbi.nlm.nih.gov/nuccore/KC663620.1, then we identified the mtDNA positions that

1127   differ from the BL6 reference genome. Finally, on these different positions, the heteroplasmy H

46

1128   was computed as explained above. The values of heteroplasmy we found with our

1129   computational analysis were very close to those estimated by ARMS-qPCR (~17% from RNA-

1130   seq data vs ~21% measured by ARMS-qPCR; and ~93% from RNA-seq data vs ~97% by

1131   measured by ARMS-qPCR).

1132   **Common features of scRNA-seq and bulk RNA-seq datasets**

1133   Differential expression analysis between the co-cultured winner HB(24%) and loser cell line

1134   BG(95%) was performed using the package EdgeR version 3.20.9 [73].

1135   Batches were specified in the argument of the function model.matrix. We fitted a quasi-likelihood

1136   negative binomial generalized log-linear model (with the function glmQLFit) to the genes that

1137   were filtered by the function filterByExpr (with default parameter). These genes were used as

1138   background for the gene enrichment analysis.

1139   We set a FDR of 0.001 as a threshold for significance. The enrichment analysis for both the

1140   scRNA-seq and bulk RNA-seq datasets were performed using the tool g:Profiler [74]. The list of

1141   up-regulated, down-regulated and background genes related to the DE analysis for the bulk

1142   RNA-seq dataset are provided in the Supplementary Tables 5, 6 and 7.

1143   **Quantification and Statistical Analysis**

1144   Box plots show lower quartile (Q1, 25th percentile), median (Q2, 50th percentile) and upper

1145   quartile (Q3, 75th percentile). Box length refers to interquartile range (IQR, Q3-Q1). The upper

1146   whisker marks the minimum between the maximum value in the dataset and the IQR times 1.5

1147   from Q3 (Q3+1.5 x IQR), while the lower whisker marks the maximum between the minimum

1148   value in the dataset and IQR times 1.5 from Q1 (Q1-1.5 x IQR). Outliers are shown outside the

1149   interval defined by box and whiskers as individual points.

1150   Flow cytometry data was analysed with FlowJo Software.

1151   Western blot quantification was performed using Image Studio Lite (LI-COR). Protein expression

1152   levels were normalised to loading controls vinculin or α-tubulin.

1153   The quantification of the DDIT3 and OPA1 expression in embryos was done by two distinct

1154   methods. DDIT3 expression was quantified by counting the number of epiblast cells with positive

47

1155   staining in the embryos of each group. The expression of OPA1 was quantified on Fiji software

1156   as the mean fluorescence across a 10 pixel width line drawn on the basal cytoplasm of each cell

1157   with high or low p-rpS6 fluorescence intensity, as specified in[7]. min of 8 cells were quantified per

1158   condition (high vs low mTOR activity) in each embryo. Six embryos treated with CI were

1159   analysed. Mean grey values of OPA1 fluorescence for each epiblast cell are pooled on the same

1160   graph.

1161   Normalisation of data from metabolic flux analysis with Seahorse was performed using Wave

1162   Desktop software (Agilent Technologies, UK) and data exported to Prism 8 (GraphPad) for

1163   statistical analysis.

1164   The statistical analysis of the results was performed using GraphPad Prism version 8.0.0 for

1165   Mac (GraphPad Software, San Diego, California USA). Data was tested for normality using

1166   Shapiro-Wilk normality test. Parametric or non-parametric statistical tests were applied

1167   accordingly. Details about the test used in each of the experiments are specified in figure

1168   legends. Statistical significance was considered with a confidence interval of 0.05%. n.s., non-

1169   significant; * $p<0.05$; ** $p<0.01$;*** $p<0.001$.

1170   **Data Availability**

1171   Data were analysed with standard programs and packages, as detailed above. Authors can

1172   confirm that all relevant data are included in the paper and/ or its supplementary information

1173   files. Source data for Figures 2-5,7 and for Extended Data Figures 4-5, 7-8 are provided with

1174   the paper. RNA-seq raw as well as processed data are available through ArrayExpress,

1175   accession numbers E-MTAB-8640, for scRNA-seq data, and E-MTAB-8692, for bulk RNA-seq

1176   data.

1177

1178   **Code Availability**

1179   All code that was used in this study is available upon request.
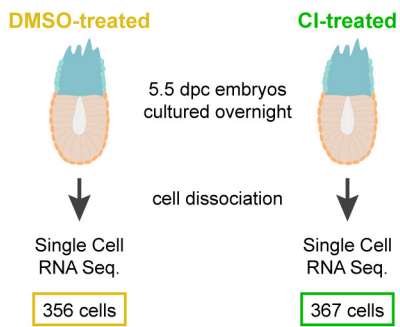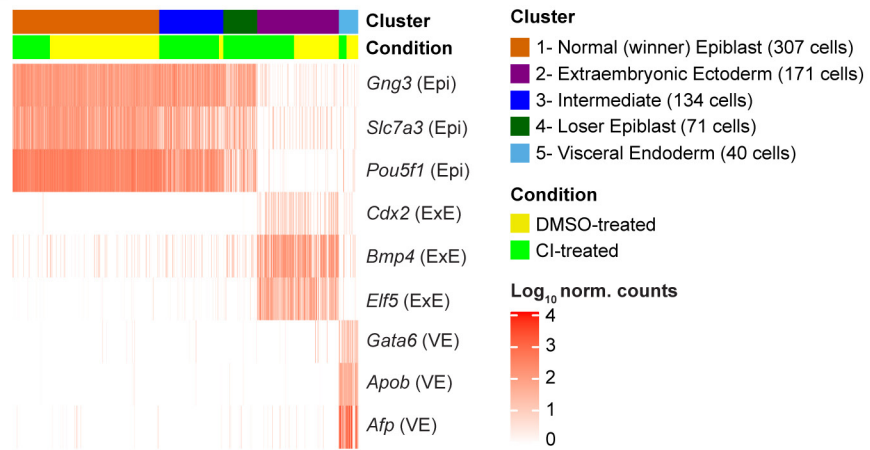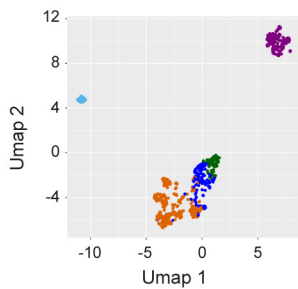
48

References

1. Bowling, S., Lawlor, K. & Rodriguez, T.A. Cell competition: the winners and losers of fitness selection. *Development* **146** (2019).

2. Diaz-Diaz, C. & Torres, M. Insights into the quantitative and dynamic aspects of Cell Competition. *Curr Opin Cell Biol* **60**, 68-74 (2019).

3. Madan, E., Gogna, R. & Moreno, E. Cell competition in development: information from flies and vertebrates. *Curr Opin Cell Biol* **55**, 150-157 (2018).

4. Morata, G. & Ripoll, P. Minutes: mutants of drosophila autonomously affecting cell division rate. *Dev Biol* **42**, 211-221 (1975).

5. Claveria, C., Giovinazzo, G., Sierra, R. & Torres, M. Myc-driven endogenous cell competition in the early mammalian embryo. *Nature* **500**, 39-44 (2013).

6. Sancho, M. *et al.* Competitive interactions eliminate unfit embryonic stem cells at the onset of differentiation. *Dev Cell* **26**, 19-30 (2013).

7. Bowling, S. *et al.* P53 and mTOR signalling determine fitness selection through cell competition during early mouse embryonic development. *Nat Commun* **9**, 1763 (2018).

8. Diaz-Diaz, C. *et al.* Pluripotency Surveillance by Myc-Driven Competitive Elimination of Differentiating Cells. *Dev Cell* **42**, 585-599 e584 (2017).

9. Hashimoto, M. & Sasaki, H. Epiblast Formation by TEAD-YAP-Dependent Expression of Pluripotency Factors and Competitive Elimination of Unspecified Cells. *Dev Cell* **50**, 139-154 e135 (2019).

10. Lima, A., Burgstaller, J., Sanchez-Nieto, J.M. & Rodriguez, T.A. The Mitochondria and the Regulation of Cell Fitness During Early Mammalian Development. *Curr Top Dev Biol* **128**, 339-363 (2018).

11. Zhou, W. *et al.* HIF1alpha induced switch from bivalent to exclusively glycolytic metabolism during ESC-to-EpiSC/hESC transition. *EMBO J* **31**, 2103-2116 (2012).

12. Khrapko, K. *et al.* Mitochondrial mutational spectra in human cells and tissues. *Proc Natl Acad Sci U S A* **94**, 13798-13803 (1997).

13. Allio, R., Donega, S., Galtier, N. & Nabholz, B. Large Variation in the Ratio of Mitochondrial to Nuclear Mutation Rate across Animals: Implications for Genetic Diversity and the Use of Mitochondrial DNA as a Molecular Marker. *Mol Biol Evol* **34**, 2762-2772 (2017).

14. Burgstaller, J.P., Johnston, I.G. & Poulton, J. Mitochondrial DNA disease and developmental implications for reproductive strategies. *Mol Hum Reprod* **21**, 11-22 (2015).

15. Gorman, G.S. *et al.* Mitochondrial diseases. *Nat Rev Dis Primers* **2**, 16080 (2016).

16. Burgstaller, J.P. *et al.* MtDNA segregation in heteroplasmic tissues is common in vivo and modulated by haplotype differences and developmental stage. *Cell Rep* **7**, 2031-2041 (2014).

17. Johnston, I.G. *et al.* Stochastic modelling, Bayesian inference, and new in vivo measurements elucidate the debated mtDNA bottleneck mechanism. *Elife* **4**, e07464 (2015).

18. Latorre-Pellicer, A. *et al.* Regulation of Mother-to-Offspring Transmission of mtDNA Heteroplasmy. *Cell Metab* (2019).

19. Lee, H.S. *et al.* Rapid mitochondrial DNA segregation in primate preimplantation embryos precedes somatic and germline bottleneck. *Cell Rep* **1**, 506-515 (2012).

20. Zhang, H., Burr, S.P. & Chinnery, P.F. The mitochondrial DNA genetic bottleneck: inheritance and beyond. *Essays Biochem* **62**, 225-234 (2018).
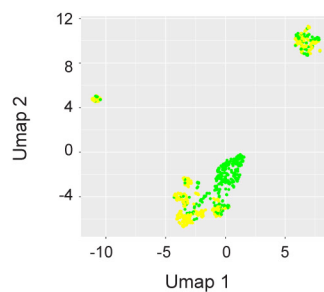
21. Sharpley, M.S. *et al.* Heteroplasmy of mouse mtDNA is genetically unstable and results in altered behavior and cognition. *Cell* **151**, 333-343 (2012).

22. Wolf, F.A. *et al.* PAGA: graph abstraction reconciles clustering with trajectory inference through a topology preserving map of single cells. *Genome Biol* **20**, 59 (2019).

23. Angerer, P. *et al.* destiny: diffusion maps for large-scale single-cell data in R. *Bioinformatics* **32**, 1241-1243 (2016).

24. Kramer, A., Green, J., Pollard, J., Jr. & Tugendreich, S. Causal analysis approaches in Ingenuity Pathway Analysis. *Bioinformatics* **30**, 523-530 (2014).

25. Haghverdi, L., Buttner, M., Wolf, F.A., Buettner, F. & Theis, F.J. Diffusion pseudotime robustly reconstructs lineage branching. *Nature methods* **13**, 845-848 (2016).

26. Cheng, S. *et al.* Single-Cell RNA-Seq Reveals Cellular Heterogeneity of Pluripotency Transition and X Chromosome Dynamics during Early Mouse Development. *Cell Rep* **26**, 2593-2607 e2593 (2019).

27. Topf, U., Wrobel, L. & Chacinska, A. Chatty Mitochondria: Keeping Balance in Cellular Protein Homeostasis. *Trends Cell Biol* **26**, 577-586 (2016).

28. Melber, A. & Haynes, C.M. UPR(mt) regulation and output: a stress response mediated by mitochondrial-nuclear communication. *Cell Res* **28**, 281-295 (2018).

29. Munch, C. The different axes of the mammalian mitochondrial unfolded protein response. *BMC Biol* **16**, 81 (2018).

30. Zhao, Q. *et al.* A mitochondrial specific stress response in mammalian cells. *EMBO J* **21**, 4411-4419 (2002).

31. Nargund, A.M., Pellegrino, M.W., Fiorese, C.J., Baker, B.M. & Haynes, C.M. Mitochondrial import efficiency of ATFS-1 regulates mitochondrial UPR activation. *Science* **337**, 587-590 (2012).

32. Quiros, P.M., Mottis, A. & Auwerx, J. Mitonuclear communication in homeostasis and stress. *Nat Rev Mol Cell Biol* **17**, 213-226 (2016).

33. Mouchiroud, L. *et al.* The NAD(+)/Sirtuin Pathway Modulates Longevity through Activation of Mitochondrial UPR and FOXO Signaling. *Cell* **154**, 430-441 (2013).

34. Saveljeva, S. *et al.* Endoplasmic reticulum stress-mediated induction of SESTRIN 2 potentiates cell survival. *Oncotarget* **7**, 12254-12266 (2016).

35. Yun, J. & Finkel, T. Mitohormesis. *Cell Metab* **19**, 757-766 (2014).

36. Chen, H. *et al.* Mitofusins Mfn1 and Mfn2 coordinately regulate mitochondrial fusion and are essential for embryonic development. *J Cell Biol* **160**, 189-200 (2003).

37. Prudent, J. & McBride, H.M. The mitochondria-endoplasmic reticulum contact sites: a signalling platform for cell death. *Curr Opin Cell Biol* **47**, 52-63 (2017).

38. Smirnova, E., Griparic, L., Shurland, D.L. & van der Bliek, A.M. Dynamin-related protein Drp1 is required for mitochondrial division in mammalian cells. *Mol Biol Cell* **12**, 2245-2256 (2001).

39. Favaro, G. *et al.* DRP1-mediated mitochondrial shape controls calcium homeostasis and muscle mass. *Nat Commun* **10**, 2576 (2019).

40. Quiros, P.M. *et al.* Multi-omics analysis identifies ATF4 as a key regulator of the mitochondrial stress response in mammals. *J Cell Biol* **216**, 2027-2045 (2017).

41. Restelli, L.M. *et al.* Neuronal Mitochondrial Dysfunction Activates the Integrated Stress Response to Induce Fibroblast Growth Factor 21. *Cell Rep* **24**, 1407-1414 (2018).

42. Richter, U. *et al.* A mitochondrial ribosomal and RNA decay pathway blocks cell proliferation. *Curr Biol* **23**, 535-541 (2013).

43. Moullan, N. *et al.* Tetracyclines Disturb Mitochondrial Function across Eukaryotic Models: A Call for Caution in Biomedical Research. *Cell Rep* **10**, 1681-1691 (2015).

44. Kauppila, J.H.K. *et al.* A Phenotype-Driven Approach to Generate Mouse Models with Pathogenic mtDNA Mutations Causing Mitochondrial Disease. *Cell Rep* **16**, 2980-2990 (2016).

45. Fan, W. *et al.* A mouse model of mitochondrial disease reveals germline selection against severe mtDNA mutations. *Science* **319**, 958-962 (2008).

46. Stewart, J.B. *et al.* Strong purifying selection in transmission of mammalian mitochondrial DNA. *PLoS Biol* **6**, e10 (2008).

47. Freyer, C. *et al.* Variation in germline mtDNA heteroplasmy is determined prenatally but modified during subsequent transmission. *Nat Genet* **44**, 1282-1285 (2012).

48. Ludwig, L.S. *et al.* Lineage Tracing in Humans Enabled by Mitochondrial Mutations and Single-Cell Genomics. *Cell* **176**, 1325-1339 e1322 (2019).

49. Chinnery, P.F. & Hudson, G. Mitochondrial genetics. *Br Med Bull* **106**, 135-159 (2013).

50. Floros, V.I. *et al.* Segregation of mitochondrial DNA heteroplasmy through a developmental genetic bottleneck in human embryos. *Nat Cell Biol* **20**, 144-151 (2018).

51. Burr, S.P., Pezet, M. & Chinnery, P.F. Mitochondrial DNA Heteroplasmy and Purifying Selection in the Mammalian Female Germ Line. *Dev Growth Differ* **60**, 21-32 (2018).

52. Rajasimha, H.K., Chinnery, P.F. & Samuels, D.C. Selection against pathogenic mtDNA mutations in a stem cell population leads to the loss of the 3243A-->G mutation in blood. *Am J Hum Genet* **82**, 333-343 (2008).

53. Ellis, S.J. *et al.* Distinct modes of cell competition shape mammalian tissue morphogenesis. *Nature* **569**, 497-502 (2019).

54. Kucinski, I., Dinan, M., Kolahgar, G. & Piddini, E. Chronic activation of JNK JAK/STAT and oxidative stress signalling causes the loser cell status. *Nat Commun* **8**, 136 (2017).

55. Kon, S. *et al.* Cell competition with normal epithelial cells promotes apical extrusion of transformed cells through metabolic changes. *Nat Cell Biol* **19**, 530-541 (2017).

56. Scialdone, A. *et al.* Resolving early mesoderm diversification through single-cell expression profiling. *Nature* **535**, 289-293 (2016).

57. Zappia, L. & Oshlack, A. Clustering trees: a visualization for evaluating clusterings at multiple resolutions. *GigaScience* **7**, giy083 (2018).

58. Scialdone, A. *et al.* Computational assignment of cell-cycle stage from single-cell transcriptome data. *Methods* **85**, 54-61 (2015).

59. Fischer, M. Census and evaluation of p53 target genes. *Oncogene* **36**, 3943-3956 (2017).

60. Ran, F.A. *et al.* Genome engineering using the CRISPR-Cas9 system. *Nat Protoc* **8**, 2281-2308 (2013).

61. Czechanski, A. *et al.* Derivation and characterization of mouse embryonic stem cells from permissive and nonpermissive strains. *Nat Protoc* **9**, 559-574 (2014).

62. Schindelin, J. *et al.* Fiji: an open-source platform for biological-image analysis. *Nat Methods* **9**, 676-682 (2012).

63. Kim, D. *et al.* TopHat2: accurate alignment of transcriptomes in the presence of insertions, deletions and gene fusions. *Genome Biol* **14**, R36 (2013).

64. Liao, Y., Smyth, G.K. & Shi, W. The R package Rsubread is easier, faster, cheaper and better for alignment and quantification of RNA sequencing reads. *Nucleic Acids Res* **47**, e47 (2019).

65. Love, M.I., Huber, W. & Anders, S. Moderated estimation of fold change and dispersion for RNA-seq data with DESeq2. *Genome Biol* **15**, 550 (2014).

66. Mootha, V.K. *et al.* PGC-1alpha-responsive genes involved in oxidative phosphorylation are coordinately downregulated in human diabetes. *Nat Genet* **34**, 267-273 (2003).

67. Subramanian, A. *et al.* Gene set enrichment analysis: a knowledge-based approach for interpreting genome-wide expression profiles. *Proc Natl Acad Sci U S A* **102**, 15545-15550 (2005).

1325   68.   Picelli, S. *et al.* Smart-seq2 for sensitive full-length transcriptome profiling in single cells.
1326   *Nat Methods* **10**, 1096-1098 (2013).
1327   69.   Patro, R., Duggal, G., Love, M.I., Irizarry, R.A. & Kingsford, C. Salmon provides fast
1328   and bias-aware quantification of transcript expression. *Nat Methods* **14**, 417-419 (2017).
1329   70.   Lun, A.T., McCarthy, D.J. & Marioni, J.C. A step-by-step workflow for low-level
1330   analysis of single-cell RNA-seq data with Bioconductor. *F1000Res* **5**, 2122 (2016).
1331   71.   Wolf, F.A., Angerer, P. & Theis, F.J. SCANPY: large-scale single-cell gene expression
1332   data analysis. *Genome Biol* **19**, 15 (2018).
1333   72.   Dobin, A. *et al.* STAR: ultrafast universal RNA-seq aligner. *Bioinformatics* **29**, 15-21
1334   (2013).
1335   73.   Robinson, M.D., McCarthy, D.J. & Smyth, G.K. edgeR: a Bioconductor package for
1336   differential expression analysis of digital gene expression data. *Bioinformatics* **26**, 139-
1337   140 (2010).
1338   74.   Reimand, J., Arak, T. & Vilo, J. g:Profiler--a web server for functional interpretation of
1339   gene lists (2011 update). *Nucleic Acids Res* **39**, W307-315 (2011).
1340

Fig. 1

a

DMSO-treated   CI-treated

5.5 dpc embryos cultured overnight

cell dissociation

Single Cell RNA Seq.

356 cells

Single Cell RNA Seq.

367 cells

b

Cluster

Condition

Gng3 (Epi)
Slc7a3 (Epi)
Pou5f1 (Epi)
Cdx2 (ExE)
Bmp4 (ExE)
Elf5 (ExE)
Gata6 (VE)
Apob (VE)
Afp (VE)

Cluster
1- Normal (winner) Epiblast (307 cells)
2- Extraembryonic Ectoderm (171 cells)
3- Intermediate (134 cells)
4- Loser Epiblast (71 cells)
5- Visceral Endoderm (40 cells)

Condition
DMSO-treated
CI-treated

Log_{10} norm. counts
4
3
2
1
0

c

Umap 2

Umap 1

Clusters:
- 1- Normal (winner) Epiblast (78 CI, 229 DMSO)
- 2- Extraembryonic Ectoderm (77 CI, 94 DMSO)
- 3- Intermediate (125 CI, 9 DMSO)
- 4- Loser Epiblast (71 CI, 0 DMSO)
- 5- Visceral Endoderm (16 CI, 24 DMSO)

d

Umap 2

Umap 1

Conditions
- DMSO-treated (356 cells)
- CI-treated (367 cells)

e

Epiblast cells (512)

Cluster 1 - Normal
Cluster 3 - Intermediate
Cluster 4 - Loser

DMSO / CI

Enrichment
3
2
1
0

Fig. 2

a

DC2 vs DC1 scatter plot

Clusters:
- 1- Normal (winner) Epiblast
- 3- Intermediate
- 4- Loser Epiblast

b

Molecular and Cellular Functions		p-value range	# Molecules
Cell Death and Survival		1.90E-02 – 1.32E-14	1181
Protein Synthesis		1.76E-02 – 2.65E-14	743
RNA Damage and Repair		1.59E-06 – 2.44E-12	137
Nucleic Acid Metabolism		1.54E-02 – 2.52E-09	220
Small Molecule Biochemistry		1.84E-02 – 1.20E-08	518

-log (p-value)   1 2 3 4 5 6 7 8 9

c

Upstream Regulator	Molecule Type	Experimental FDR	p-value of overlap
RICTOR	other	9.3E-04	3.5E-33
TLE3	other	-	1.2E-18
MYC	transcription regulator	-	1.1E-16
MYCN	transcription regulator	2.3E-10	5.6E-16
TP53	transcription regulator	-	3.8E-13
IGF1R	transmembrane receptor	-	1.1E-12
STK11	kinase	-	4.0E-12
NFE2L2	transcription regulator	1.6E-10	7.8E-12
INSR	kinase	-	1.2E-11
LONP1	peptidase	1.1E-06	2.7E-11

d

DC2 vs DC1 with Losing score scale (0, 0.46, 0.93, 1.4, 1.9)

e

CI-treated (274 cells)   DMSO-treated (238 cells)

Losing Score vs Clusters

Clusters:
- 1- Normal (winner) Epiblast
- 3 - Intermediate
- 4 - Loser Epiblast

f

Condition
Cluster
Losing score

Klf4*
Klf5*
Sox2
Pou3f1
Tcf7l1*
Pou5f1*
Rex1
} Naïve Pluripotency

Fgf5*
Tdgf1*
} Primed Pluripotency

Mesp1
T
} Mesoderm

Neurod1*
Sox1
} Neuroectoderm

Sox17*
Gata6
} Endoderm

Condition
- CI-treated

Cluster
- 1- Normal (winner) Epiblast
- 3- Intermediate
- 4- Loser Epiblast

Losing score
2
1.5
1
0.5
0

Log$_{10}$ norm. counts
3
2
1
0

Fig. 3

a Percentage / -log (p-value) bar chart

Mitochondrial Dysfunction — 144
Oxidative Phosphorylation — 95
EIF2 Signalling — 169

Legend:
- Overlaps with dataset
- No overlap with dataset
- -log (p-value)

b Mitochondrial inner membrane electron transport chain diagram

Outer Mitochondrial Membrane / Cytoplasm / Intermembrane Space / Inner Mitochondrial Membrane / Mitochondrial Matrix

Complex I, Complex II, Complex III, Complex IV, Complex V

Legend:
- Down-regulated gene
- Up-regulated gene
- Gene did not pass analysis cut-off
- Gene not part of experimental dataset

c

Electron Transport Chain

mt-Atp6, *mt-Nd3* ($\log_{10}$ norm. counts vs Losing score)

Mitochondria Membrane and Cristae Organization

Opa1, *Samm50* ($\log_{10}$ norm. counts vs Losing score)

d DMSO-treated / CI-treated

5.5 dpc embryos cultured overnight

Immunostaining

or

isolation of epiblasts *

cell dissociation and analysis of ΔΨm

50 X

e Hoechst OPA1 p-rpS6

Merged / Detail inset / OPA1 / p-rpS6 — 20 µm

f Mean OPA1 fluorescence (mean grey value) vs Low p-rpS6 / High p-rpS6 (***)

g DMSO CI — Normalized To Mode vs TMRM; Low TMRM / High TMRM

h Frequency of total cell population (%) — High TMRM / Low TMRM, DMSO vs CI (***)

Fig. 4

a

TCA Cycle Metabolite Enrichment - Differentiation (day 3)

b

Mitochondria Stress Test - Differentiation (day 3)

□ Wild-type   ● Bmpr1a⁻/⁻

c

□ Wild-type   ▨ Bmpr1a⁻/⁻

d

Glycolysis Stress Test - Differentiation (day 3)

□ Wild-type   ● Bmpr1a⁻/⁻

e

□ Wild-type   ▨ Bmpr1a⁻/⁻

Δψm and Mitochondrial mass - Differentiation (day 3)

f

Separate culture   Co-culture

Wild-type Bmpr1a⁻/⁻

□ Wild-type ▨ Bmpr1a⁻/⁻

g

Separate culture   Co-culture

Wild-type 4n

□ Wild-type ▨ 4n

h

Hoechst | Bmpr1a⁻/⁻ - GFP | Mitotracker Red | Merged

Hoechst | Bmpr1a⁻/⁻ - GFP | TOMM20 | Merged

i

j

k

Fig. 5

Mitochondrial shape - Pluripotency

a

Mfn2⁻/⁻ Wild-type *Drp1⁻/⁻*

Hoechst TOMM20 NANOG

Cell competition assays

b

Pluripotency

Wild-type *Mfn2⁻/⁻*

Final / Initial cell numbers

Separate Co-culture

c

Differentiation (day 3)

Wild-type *Drp1⁻/⁻*

Final / Initial cell numbers

Separate Co-culture

Metabolic profile of *Mfn2⁻/⁻* cells - Pluripotency

d

Δψm in Separate culture

Wild-type *Mfn2⁻/⁻*

Normalized To Mode

TMRM

Fold change (MFI vs control)

Wild-type *Mfn2⁻/⁻*

e

Mitochondria Stress Test

Wild-type *Mfn2⁻/⁻*

Pyr 1 mM OM 2.5 µM FCCP 300 nM R&A 6 µM

OCR (pmol O_2/min) per 100 000 cells

Time (minutes)

OCR (pmol O_2/min) per 100 000 cells

Basal Respiration Maximal Respiration ATP production

Metabolic profile of *Drp1⁻/⁻* cells - Differentiation (day 3)

f

Δψm in Separate culture

Wild-type *Drp1⁻/⁻*

Normalized To Mode

TMRM

Fold change (MFI vs control)

Wild-type *Drp1⁻/⁻*

g

Mitochondria Stress Test

Wild-type *Drp1⁻/⁻*

Pyr 1 mM OM 2.5 µM FCCP 300 nM R&A 6 µM
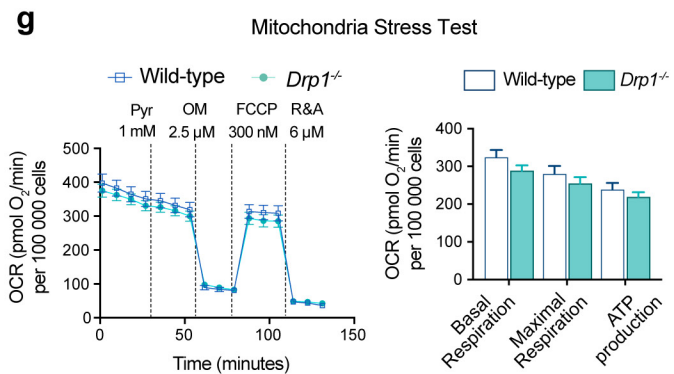
OCR (pmol O_2/min) per 100 000 cells

Time (minutes)

OCR (pmol O_2/min) per 100 000 cells

Basal Respiration Maximal Respiration ATP production

h

Wild-type *Drp1⁻/⁻*

50 KDa — ATF4
37 KDa — p-eIF2α
37 KDa — PCNA

ATF4 / PCNA

Wild-type *Drp1⁻/⁻*

p-eIF2α / PCNA

Wild-type *Drp1⁻/⁻*

i

Wild-type *Drp1⁻/⁻*

100 KDa — L-OPA1
75 KDa — S-OPA1
15 KDa — TOMM20
37 KDa — PCNA

TOMM20 / PCNA

Wild-type *Drp1⁻/⁻*

L-OPA1/ PCNA

Wild-type *Drp1⁻/⁻*

S-OPA1/PCNA

Wild-type *Drp1⁻/⁻*

j

Wild-type *Drp1⁻/⁻*
Con Dox Con Dox

100 KDa — L-OPA1
75 KDa — S-OPA1
50 KDa — α-tubulin

Con 22.5 µM Dox

L-OPA1/ α-tubulin

Wild-type *Drp1⁻/⁻*

S-OPA1/ α-tubulin

Wild-type *Drp1⁻/⁻*

Fig. 6

a — Heteroplasmy (all polymorphisms)
adjusted p-value = 4.9E−27

b — *mt-Rnr1* 326
adj. p-value = 3E-19

c — *mt-Rnr1* 327
adj. p-value = 5E-19

d — *mt-Rnr1* 305
adj. p-value = 2E-10

e — *mt-Rnr1* 304
adj. p-value = 1E-09

f — *mt-Rnr1* 300
adj. p-value = 2E-09

g — *mt-Rnr1* 303
adj. p-value = 6E-08

Clusters (panels a-g)
- 1 - Normal (winner) Epiblast
- 3 - Intermediate
- 4 - Loser Epiblast

h — Percentage of cells per cluster carrying significant mutations in *mt−Rnr1*

Clusters
- 1 - Normal (winner) Epiblast
- 3 - Intermediate
- 4 - Loser Epiblast

i — Spearman correlation of mutations in *mt-Rnr1* from CI-treated (215 cells)

300 *mt−Rnr1*
304 *mt−Rnr1*
305 *mt−Rnr1*
303 *mt−Rnr1*
326 *mt−Rnr1*
327 *mt−Rnr1*

Spearman correlation

Fig. 7

a 4 hybrid mouse strains containig wild-derived mtDNA variants in the nuclear DNA from C57BL/6N lab mouse

ST HB/HB BG/BG C57BL/6N "Donor"

416 / 35   107 / 13   86 / 16   0 / 0   SNPs/a.a. changes

Increasing genetic distance from C57BL/6N

mESCs derived from embryos of hybrid mice

late blastocyst (4.5 dpc)

Isolated mESCs in cell culture

Cell competition assays - Pluripotency

b HB (100%) C57BL/6N
Final / Initial cell numbers
Separate Co-culture **

c HB (24%) C57BL/6N
Final / Initial cell numbers
Separate Co-culture **

Cell competition assays - Pluripotency

d HB (24%) BG (95%)
Final / Initial cell numbers
Separate Co-culture * ***

e HB (24%) HB (100%)
Final / Initial cell numbers
Separate Co-culture

Cell death analysis during competition - Pluripotency

f Separate Co-culture
HB (24%) - GFP
BG (95%)
Hoechst HB - GFP Cleaved Caspase-3
50 μm

HB (24%) BG (95%)
% Apoptotic Events
Separate Co-culture ** **

g **Separate**
loser BG (95%) vs winner HB (24%)

Hallmarks Gene Set

INTERFERON_ALPHA_RESPONSE
INTERFERON_GAMMA_RESPONSE
KRAS_SIGNALING_UP
EPITHELIAL_MESENCHYMAL_TRANSITION
APICAL_JUNCTION
COMPLEMENT
TNFA_SIGNALING_VIA_NFKB
NOTCH_SIGNALING
COAGULATION
PANCRAS_BETA_CELLS
INFLAMMATORY_RESPONSE
MYOGENSIS
UV_RESPONSE_DN
OXIDATIVE PHOSPHORYLATION

FDR q value
0.015
0.010
0.005
0.000

no. genes in core
25
50
75

NES

h **Co-culture**
loser BG (95%) vs winner HB (24%)

Hallmarks Gene Set

INTERFERON_ALPHA_RESPONSE
INTERFERON_GAMMA_RESPONSE
KRAS_SIGNALING_UP
PANCRAS_BETA_CELLS
APICAL_JUNCTION
COAGULATION
EPITHELIAL_MESENCHYMAL_TRANSITION
UV_RESPONSE_DN
COMPLEMENT
TNFA_SIGNALING_VIA_NFKB
INFLAMMATORY_RESPONSE
NOTCH_SIGNALING
MYOGENSIS
APICAL_SURFACE
OXIDATIVE PHOSPHORYLATION
E2F_TARGETS
MYC_TARGETS_V1
UNFOLDED_PROTEIN_RESPONSE
PROTEIN_SECRETION
PIK3_AKT_MTOR_SIGNALING

FDR q value
0.03
0.02
0.01
0.00

no. genes in core
25
50
75
100

NES

Fig. 8

Mitochondria-centered Cell Fitness

Extended Data Fig. 1

a

Selection criteria for quality control (QC) of cells

QC-Good cells (723) — Log$_{10}$ total number of reads

QC-Good cells (723) — Fraction of mapped reads

QC-Good cells (723) — Fraction of genes

QC-Good cells (723) — Fraction of mt-genes

QC-Good cells (723) — Fraction of spikes

QC-Good cells (723) — Number of genes above 10 RPM

b

Condition\Batch	1	2	3	4	5
CI-treated	136	105	86	16	24
DMSO	132	110	78	15	21

c

Cluster/Batch	1	2	3	4	5
1	147	81	57	7	15
2	45	65	44	7	10
3	46	34	35	13	6
4	23	18	21	2	7
5	7	17	7	2	7

d

e
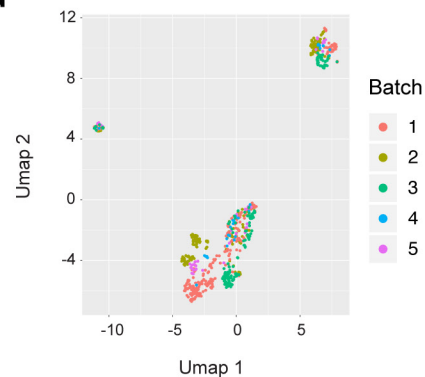
Cluster robustness
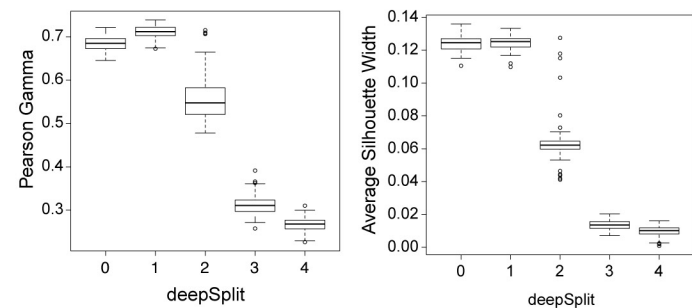
f

deepSplit clustering
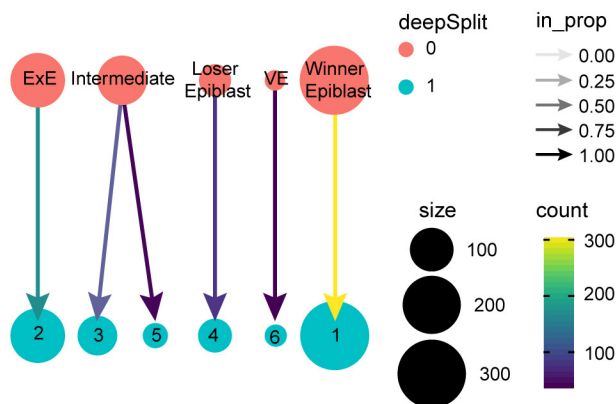
Extended Data Fig. 2

a

b

c

d

e

Extended Data Fig. 3

a

Cluster	
Condition	
Losing score	

Cluster
- Normal (winner) Epiblast
- Intermediate
- Loser Epiblast

Condition
- CI-treated

Differentially expressed genes
- Up-regulated
- Down-regulated

Losing score
2
1.5
1
0.5
0

Log₁₀ norm counts
6
4
2
0

b Targets activated by p53 (80 genes)

56.2 % 43.8 %
- Down-regulated genes
- Up-regulated genes

c Targets repressed by p53 (41 genes)

80.5 % 19.5 %
- Down-regulated genes
- Up-regulated genes

d

Naïve Pluripotency *vs* Endoderm
Spearman correlation = -0.13

Naïve Pluripotency *vs* Neureoctoderm
Spearman correlation = -0.11

Neuroectoderm *vs* Endoderm
Spearman correlation = 0.24

e

Cluster
- Epiblast 5.5
- Epiblast 6.25
- Epiblast 6.5

f

DPT244
Path and Tips
- Tips

g

Losing Score (dpt)

Clusters

CI-treated (274)	DMSO-treated (238)	Untreated (520)
Winner Epi.	Winner Epi.	Epi. E5.5
Intermediate	Intermediate	Epi. E6.25
Loser Epi.	Intermediate	Epi. E6.5

Extended Data Fig. 4

a

b

Gene	FDR	Rank
Ddit3	4.63E-39	2
Atf3	6.08E-27	22
Atf4	2.14E-23	31
Foxo3	2.69E-22	37
Ppp1r15a	8.33E-18	68
Eif2ak3	7.17E-13	150
Nfe2l2	1.55E-10	207
Gdf15	5.53E-08	333

c

Gene	FDR	Rank
Mthfd1l	2.54E-35	147
Hspe1	8.71E-34	164
Cat	2.44E-30	219
Hspd1	6.93E-13	1262
Sod2	1.25E-10	1551
Hsph1	4.48E-10	1655
Lonp1	1.08E-06	2348
Eif2a	1.49E-06	2382
Mthfd2	1.31E-05	2693
Hspa4	2.84E-05	2790
Cth	2.53E-03	3677
Nrf1	2.86E-03	3698

d
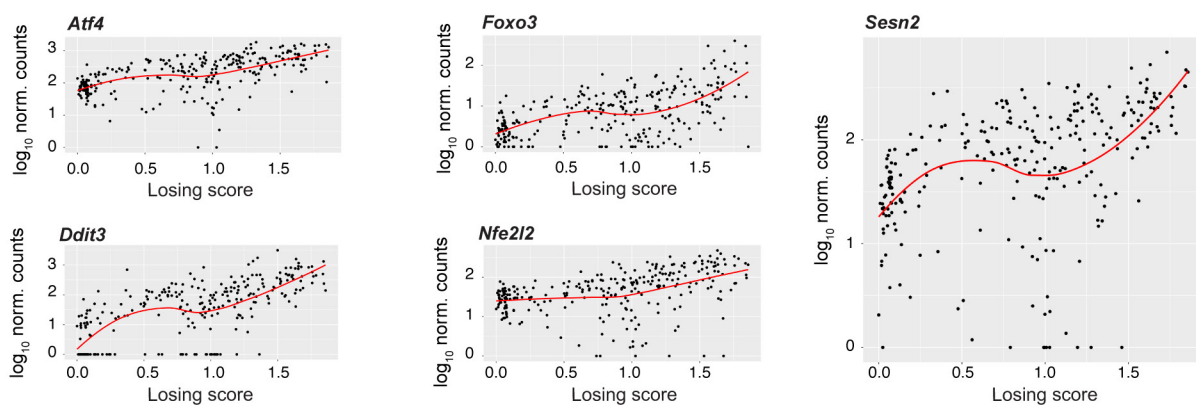
e
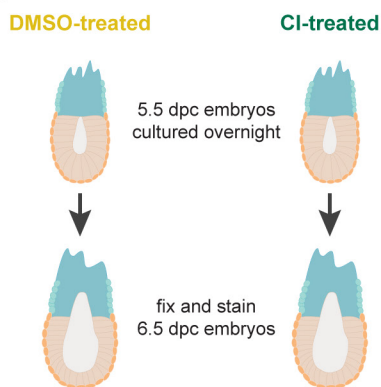
f

g
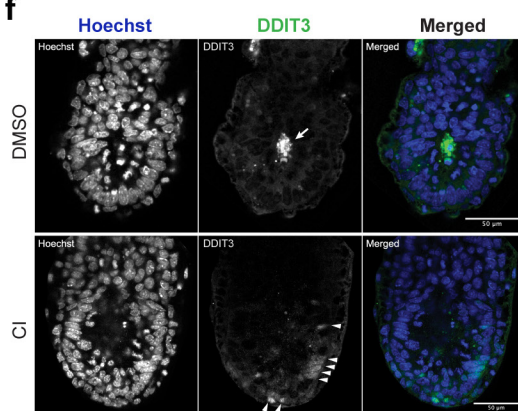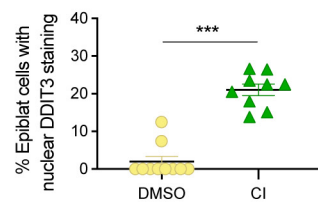
Extended Data Fig. 5

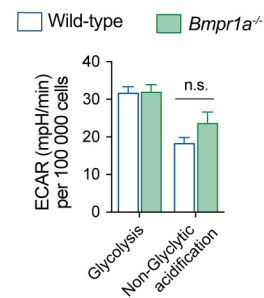**a** Mitochondria Stress Test - Pluripotency
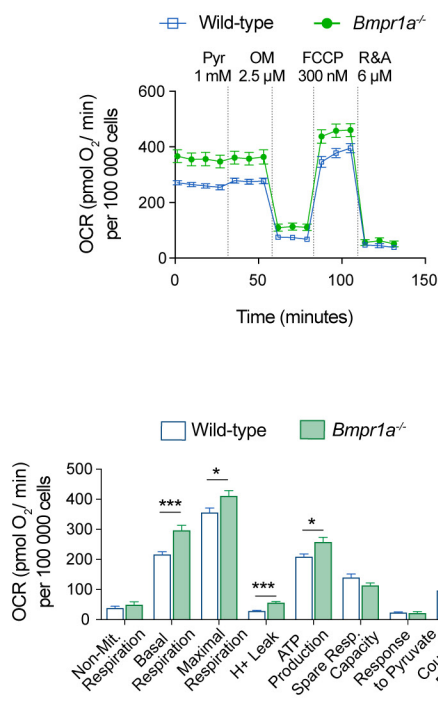
b Glycolysis Stress Test - Pluripotency
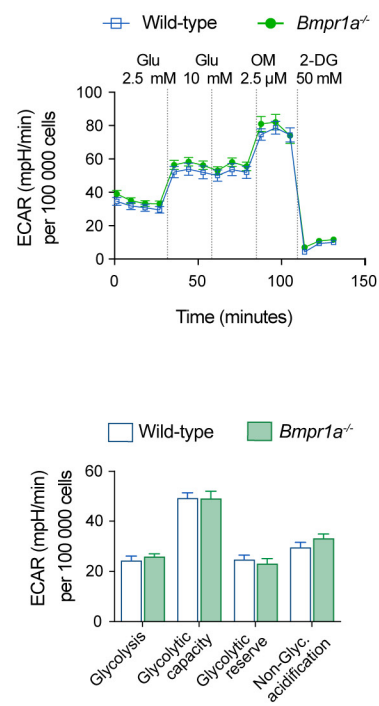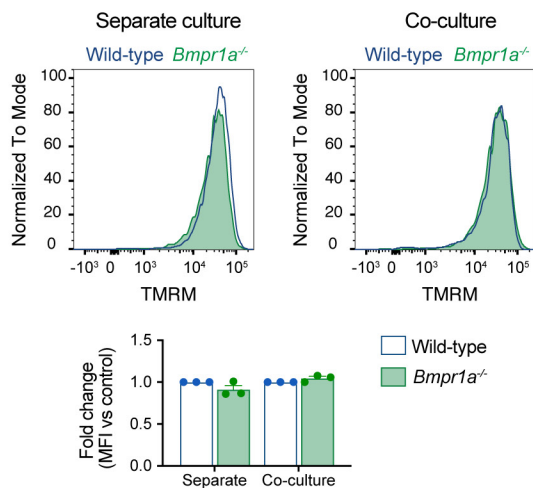

c Mitochondria Stress Test - Differentiation (day 3)
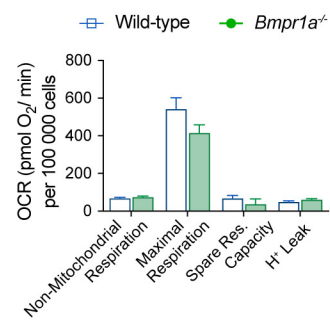
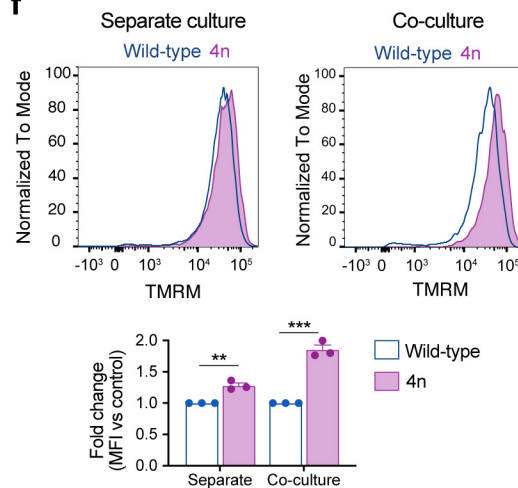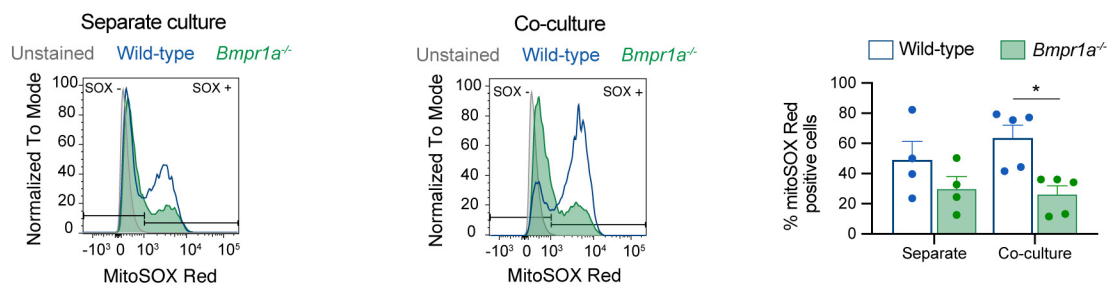**d** Glycolysis Stress Test - Differentiation (day 3)

Δψm - Pluripotency

e

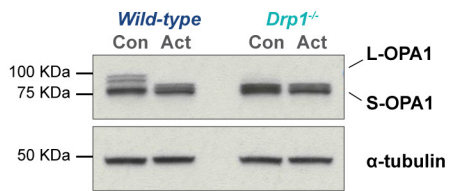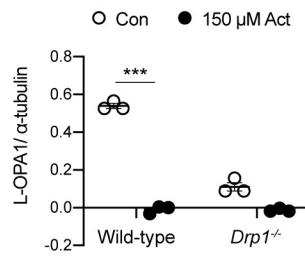**f**

Mitochondrial ROS - Differentiation (day 3)

g

Extended Data Fig. 6

Act treatment at Differentiation day 3 (6h)

a

b

c

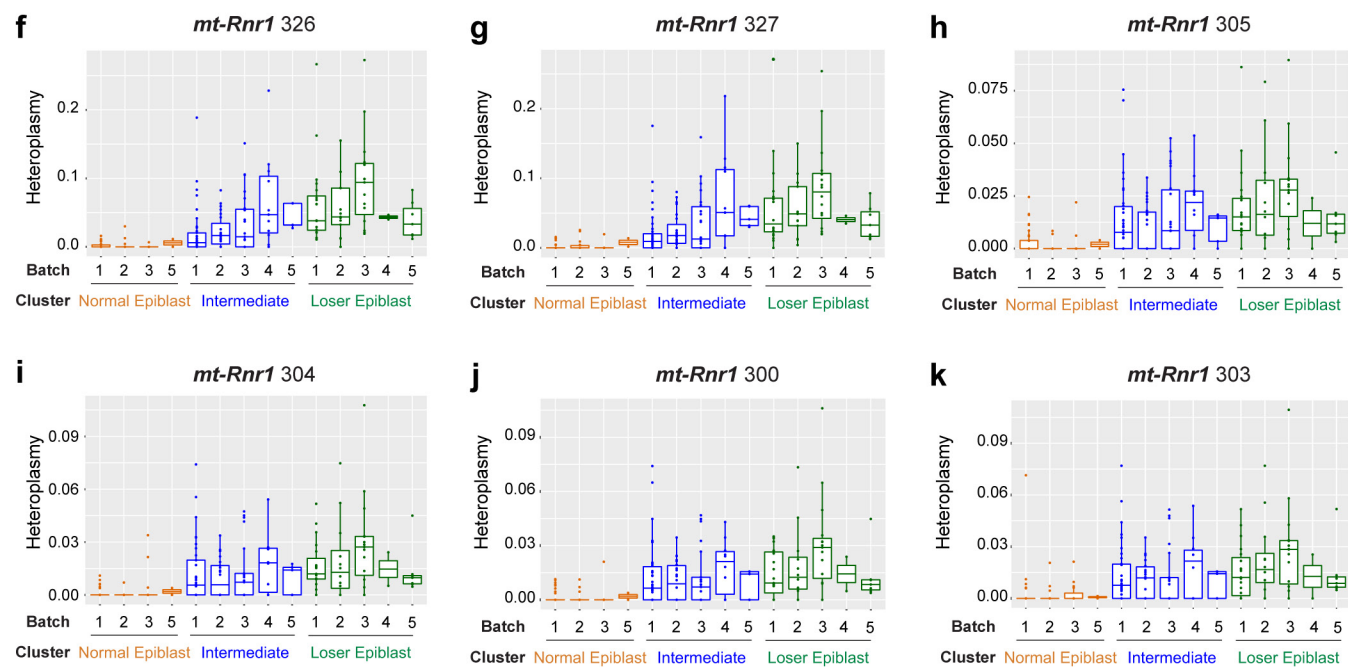# Extended Data Fig. 7

a *mt-Rnr2* 2077
adj. p-value = 2E-11

b *mt-Rnr2* 2079
adj. p-value = 3E-11

c *mt-Rnr2* 2081
adj. p-value = 3E-11

d *mt-Rnr2* 2031
adj. p-value = 2E-09

e *mt-Rnr2* 2074
adj. p-value = 3E-08

Clusters (panels A to E): 1 - Normal (winner) Epiblast   3 - Intermediate   4 - Loser Epiblast

f *mt-Rnr1* 326

g *mt-Rnr1* 327

h *mt-Rnr1* 305

i *mt-Rnr1* 304

j *mt-Rnr1* 300

k *mt-Rnr1* 303
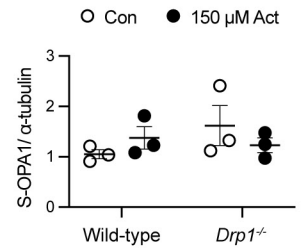
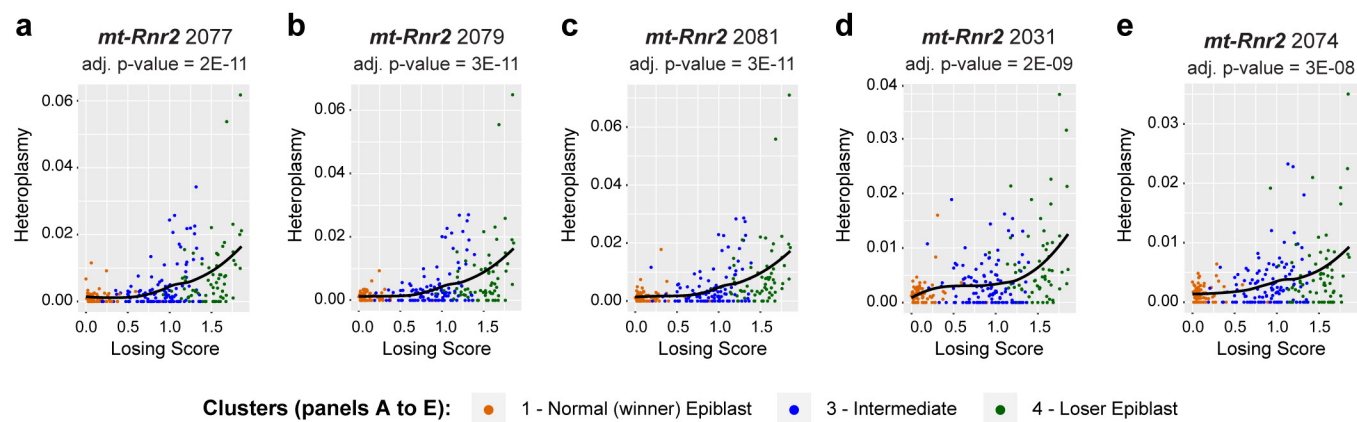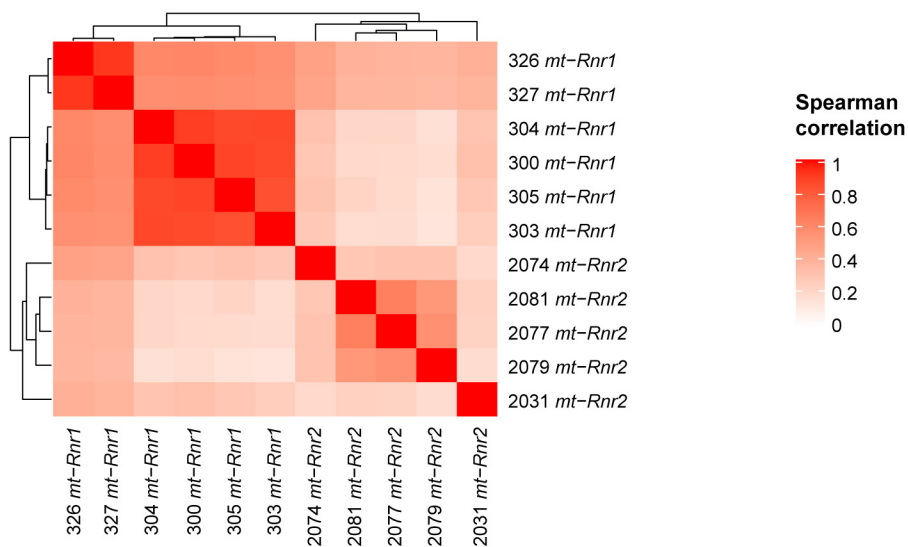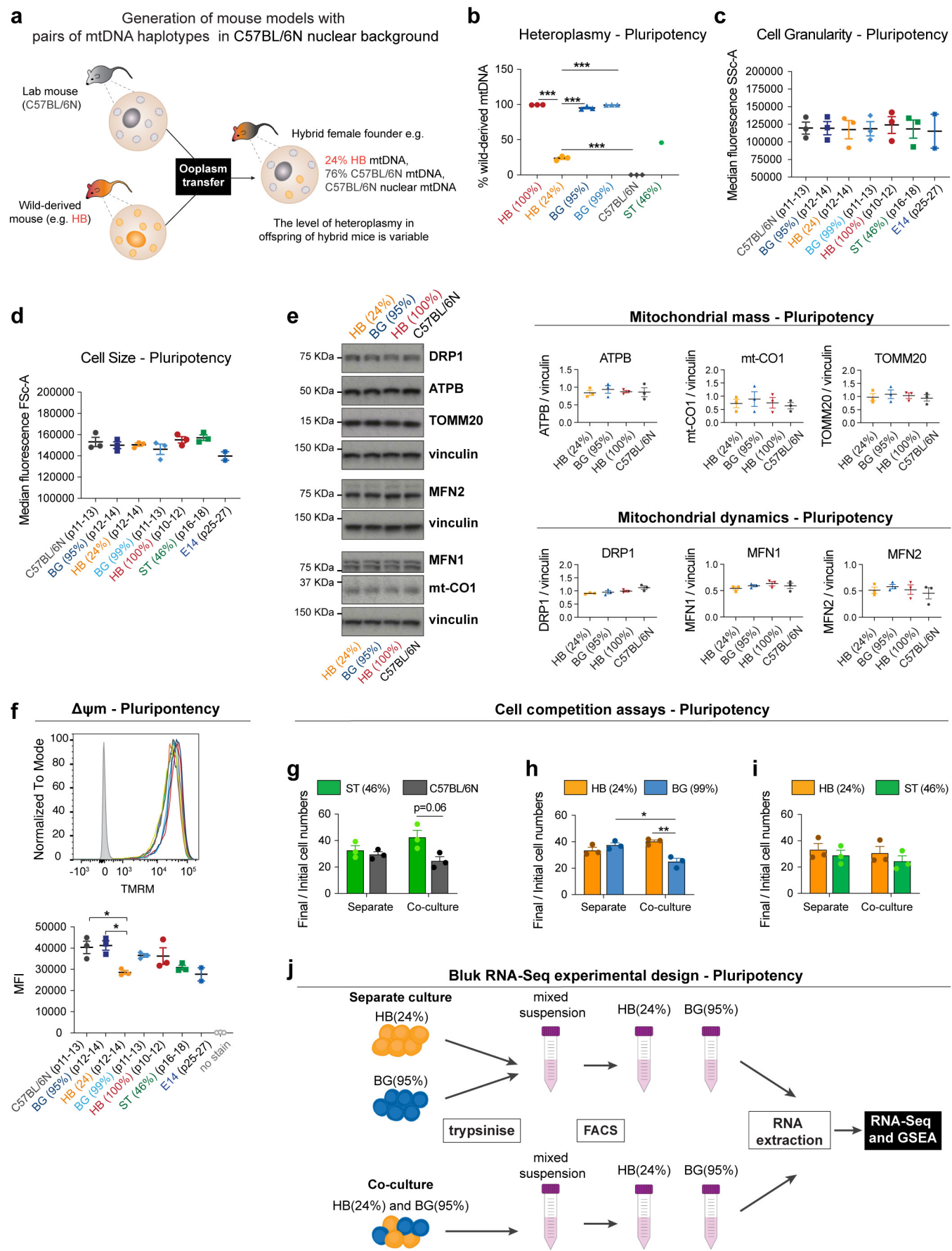**l** Spearman correlation of mutations within *mt-Rnr1* and *mt-Rnr2* from CI-treated (214 cells)

Extended Data Fig. 8

a Generation of mouse models with pairs of mtDNA haplotypes in C57BL/6N nuclear background

Lab mouse (C57BL/6N)

Wild-derived mouse (e.g. HB)

Ooplasm transfer

Hybrid female founder e.g.

24% HB mtDNA,
76% C57BL/6N mtDNA,
C57BL/6N nuclear mtDNA

The level of heteroplasmy in offspring of hybrid mice is variable

b Heteroplasmy - Pluripotency

c Cell Granularity - Pluripotency

d Cell Size - Pluripotency

e

Mitochondrial mass - Pluripotency

ATPB   mt-CO1   TOMM20

Mitochondrial dynamics - Pluripotency

DRP1   MFN1   MFN2

f Δψm - Pluripotency

Cell competition assays - Pluripotency

g ST (46%)   C57BL/6N   p=0.06

h HB (24%)   BG (99%)

i HB (24%)   ST (46%)

j Bluk RNA-Seq experimental design - Pluripotency

Separate culture
HB(24%)
BG(95%)

mixed suspension → HB(24%)   BG(95%)

trypsinise   FACS

RNA extraction → RNA-Seq and GSEA

Co-culture
HB(24%) and BG(95%)

mixed suspension → HB(24%)   BG(95%)

Extended Data Fig. 9

Mitochondria Stress Test - Pluripotency
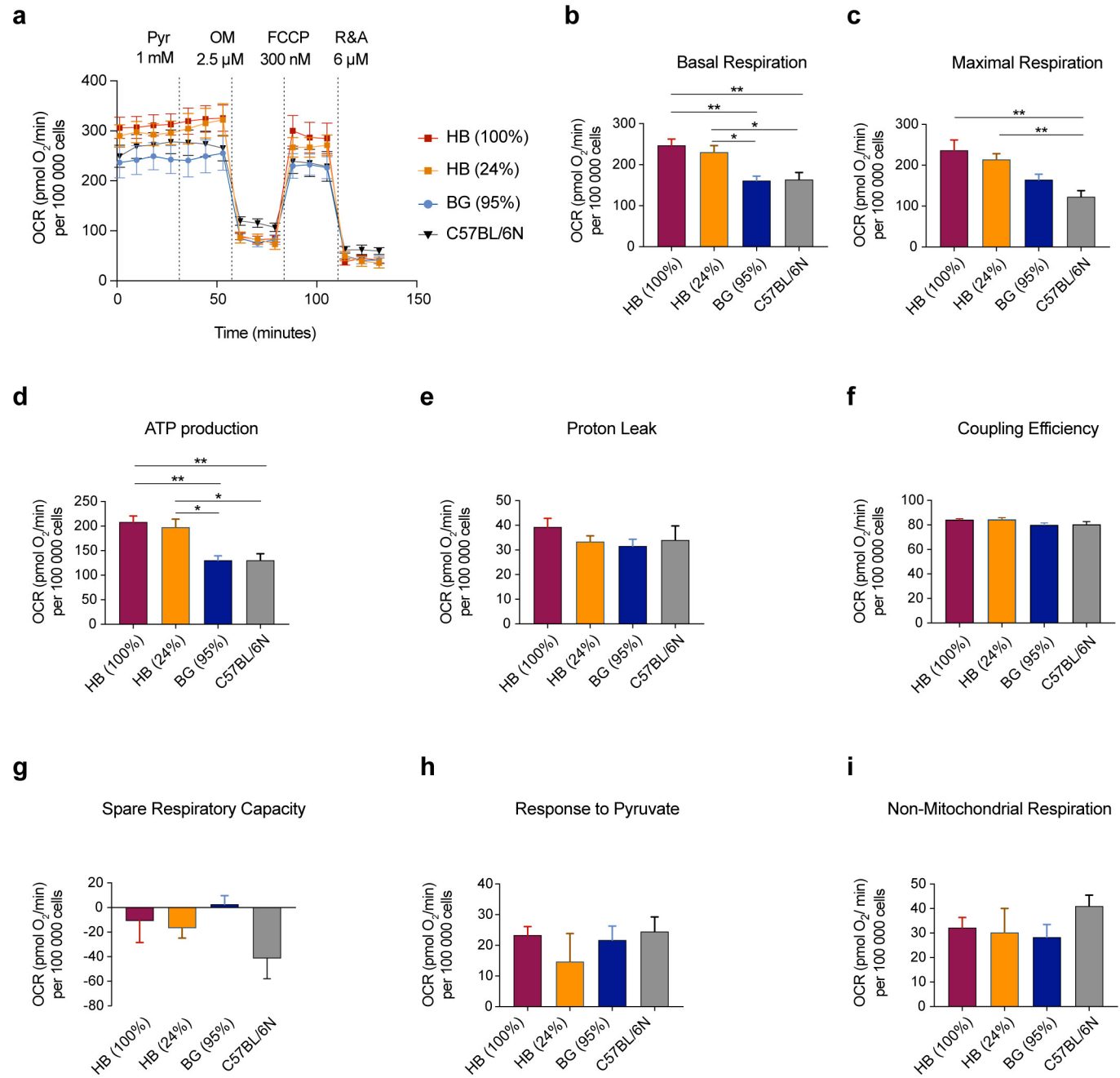
Extended Data Fig. 10

a

Source	Term	Adjusted p-value
GO:CC	mitochondrial protein complex	5.91E-05
GO:CC	inner mitochondrial membrane protein complex	8.84E-04
GO:CC	mitochondrial inner membrane	8.93E-04
GO:CC	mitochondrial respirasome	2.44E-03
GO:CC	respiratory chain complex	3.89E-03
GO:CC	respirasome	6.50E-03
GO:CC	mitochondrial part	1.06E-02
GO:CC	organelle inner membrane	4.65E-02
KEGG	oxidative phosphorylation	7.71E-04
KEGG	Huntington disease	2.35E-03
WP	electron transport chain	1.26E-03

b

c